BAŞKENT UNIVERSITY
INSTITUTE OF SCIENCE AND ENGINEERING
DEPARTMENT OF ELECTRICAL AND ELECTRONICS ENGINEERING
MASTER OF SCIENCE IN ELECTRICAL AND ELECTRONICS ENGINEERING

COMPACT DUAL-BAND BANDSTOP FILTER BY USING OPEN-LOOP RESONATORS

BY

ERAY KAPLAN

MASTER OF SCIENCE THESIS

ANKARA - 2023

BAŞKENT UNIVERSITY
INSTITUTE OF SCIENCE AND ENGINEERING
DEPARTMENT OF ELECTRICAL AND ELECTRONICS ENGINEERING
MASTER OF SCIENCE IN ELECTRICAL AND ELECTRONICS ENGINEERING

COMPACT DUAL-BAND BANDSTOP FILTER BY USING OPEN-LOOP RESONATORS

BY

ERAY KAPLAN

MASTER OF SCIENCE THESIS

ADVISOR

ASSIST. PROF. DR. HAYRULLAH YILDIZ

CO-ADVISOR

ASSIST. PROF. DR. ALPARSLAN ÇAĞRI YAPICI

ANKARA – 2023

BASKENT UNIVERSITY

INSTITUTE OF SCIENCE AND ENGINEERING

This study, which was prepared by Eray Kaplan, for the program of Master's of Electrical and Electronics Engineering with Thesis, has been approved in partial fulfillment of the requirements for the degree of MASTER OF SCIENCE in Electrical and Electronics Engineering Department by the following committee.

Date of Thesis Defense: 26 / 05 / 2023

Thesis Title: Compact Dual-Band Bandstop Filter By Using Open-Loop Resonators

Examining Commitee Members	**Signature**
Prof. Dr. Asım Egemen YILMAZ, Ankara University	……...
Assist. Prof. Dr. Hayrullah YILDIZ, Baskent University	……...
Assist. Prof. Dr. Murat ÜÇÜNCÜ, Baskent University	……...

APPROVAL

Prof. Dr. Ömer Faruk ELALDI
Director, Institute of Science and Engineering
Date : … / … / ….……

BAŞKENT ÜNİVERSİTESİ

FEN BİLİMLER ENSTİTÜSÜ

YÜKSEK LİSANS TEZ ÇALIŞMASI ORİJİNALLİK RAPORU

Tarih: ... / ... / 20...

Öğrencinin Adı, Soyadı: Eray Kaplan

Öğrencinin Numarası: 22010479

Anabilim Dalı: Elektrik/Elektronik Mühendisliği Anabilim Dalı

Programı: Elektrik/Elektronik Mühendisliği Tezli Yüksek Lisans Programı

Danışmanın Unvanı/Adı, Soyadı: Dr. Öğr. Üyesi Hayrullah YILDIZ

Tez Başlığı: Compact Dual-Band Bandstop Filter by Using Open-Loop Resonators

Yukarıda başlığı belirtilen Yüksek Lisans tez çalışmamın; Giriş, Ana Bölümler ve Sonuç Bölümünden oluşan, toplam 54 sayfalık kısmına ilişkin, 13 / 06 / 2023 tarihinde tez danışmanım tarafından Turnitin adlı intihal tespit programından aşağıda belirtilen filtrelemeler uygulanarak alınmış olan orijinallik raporuna göre, tezimin benzerlik oranı %15'dir. Uygulanan filtrelemeler:

1. Kaynakça hariç
2. Alıntılar hariç
3. Beş (5) kelimeden daha az örtüşme içeren metin kısımları hariç

"Başkent Üniversitesi Enstitüleri Tez Çalışması Orijinallik Raporu Alınması ve Kullanılması Usul ve Esaslarını" inceledim ve bu uygulama esaslarında belirtilen azami benzerlik oranlarına tez çalışmamın herhangi bir intihal içermediğini; aksinin tespit edileceği muhtemel durumda doğabilecek her türlü hukuki sorumluluğu kabul ettiğimi ve yukarıda vermiş olduğum bilgilerin doğru olduğunu beyan ederim.

Öğrenci İmzası:.....

ONAY

... / ... / 20...

Öğrenci Danışmanı

Dr. Öğr. Üyesi Hayrullah YILDIZ

ACKNOWLEDGEMENTS

I would like to express my sincere gratitude to my thesis advisor Dr. Hayrullah YILDIZ and Co-Advisor Dr. Alparslan Çağrı YAPICI for their valuable guidance, support and, encouragement throughout my research. Their expertise, patience, and insightful feedback have been crucial in the successful completion of this thesis.

I am also deeply grateful to my parents, Şaziye Eren KAPLAN, Ayhan KAPLAN, and my sister Seray KAPLAN for their encouragement and limitless support throughout my educational journey for 22 years. Their sacrifices and dedication have been an endless source of motivation and inspiration for me.

I would like to express my heartfelt appreciation to my partner, İrem ÖZKAYA, for her unwavering support, love, and understanding. Her patience and motivation have been an essential part of my success for 8 years.

Furthermore, I would like to express my thanks to my friend, Hüseyin TOKAR, for his analytical skills and unique perspective, which have added tremendous value to my research. His constructive insights and thought-provoking discussions have greatly enriched my work.

Finally, I would like to express my gratitude to my line managers, İlter KARADEDE and Cihangir ERDEM, for their support and flexibility, which enabled me to balance my work commitments with my academic pursuits.

Once again, I would like to express my heartfelt thanks to everyone who has supported me to complete my thesis.

ÖZET

ERAY KAPLAN

Açık Halka Rezonatörleri ile Kompakt Çift Bantlı Bant Durduran Filtre Tasarımı

Başkent Üniversitesi Fen Bilimleri Enstitüsü

Elektrik Elektronik Mühendisliği Bölümü

2023

Bu çalışmada ikinci dereceden çift bantlı bant durduran filtre tasarım yöntemi tanıtıldı. Durdurma bantları geniş bantlı alıcılara girişim yapan 2110 MHz – 2200 MHz ve 2500 MHz –2690 MHz aralığında olan LTE bantları seçildi. Çift bantlı bant durduran filtreyi sentezlemek için doğrudan bağlaşım matrisi sentezleme yöntemi kullanıldı. Çift bantlı filtre sentezleme yöntemi, sentezlenen tek bantlı filtre bağlaşım matrisi kullanılarak çift bantlı filtre elde edilmesi ile sadeleştirildi. Bu sadeleştirme, kare açık halka rezonatörlerinin gruplanmış halde kullanılıp iki modlu rezonatör elde edilmesi ile başarıldı. Rezonatörlerin gruplanması sonucu boyut küçültüldü ve kayıplar azaltıldı. Buna karşın, bant bastırma değeri korundu. Bağlaşım matrisi sentezlendi ve aynı matrisi kullanarak iki ayrı filtre RT/Duroid 6010 ve FR-4 alttaş malzeme üzerinde tasarlandı. RT/Duroid 6010 alttaş malzemesi kullanılarak tasarlanan filtre potansiyel yüksek RF performansı sebebiyle simülasyonlarda kullanıldı. Fakat, üretim ve ölçüm için maliyet etkin olan FR-4 alttaş malzemesi kullanılarak tasarlanan filtre seçildi. Ölçüm sonuçları tasarlanan filtrenin tasarım beklentilerini karşıladığını gösterdi.

ANAHTAR KELİMELER: Çift Bantlı Bant Durduran Filtre, Doğrudan Sentezleme Yöntemi, Açık Halka Rezonatörleri

ABSTRACT

ERAY KAPLAN

COMPACT DUAL-BAND BANDSTOP FILTER BY USING OPEN-LOOP RESONATORS

Başkent University Institute Of Science

Department Of Electrical And Electronics Engineering

2023

In this study, a second order dual-band bandstop filter design method is developed. The two LTE frequency bands 2110 MHz-2200 MHz and 2500 MHz – 2690 MHz are chosen as stopbands since wideband receivers suffers from interference in these frequency range. Direct coupling matrix synthesis technique is utilized for implementing dual-band bandstop filter. The design process of a dual-band bandstop filter is reduced by implementing the filter with a coupling matrix size of a single-band bandstop filter. In order to reduce the coupling matrix size, dual mode resonators are produced by grouping Square Open-Loop resonators (SOLR). Since the resonators have been used in groups, the size and insertion loss have been reduced while the rejection level is kept constant. The identical coupling matrix is implemented as a filter on two distinct substrates, RT/Duroid 6010 and FR4. The substrate RT/Duroid 6010 is utilized for simulations for its high RF performance potential. However, for implementation of designed filter, cost-effective FR-4 is utilized as the substrate. The measurement results of the implemented filter demonstrate that it complies with the design specifications.

KEY WORDS: Dual-Band Bandstop Filter, Direct Synthesis Method, Open-Loop Resonators

TABLE OF CONTENTS

LIST OF TABLES

LIST OF FIGURES

Page

1. INTRODUCTION

The number of users in the frequency spectrum is increasing day by day. Every new wireless standard requires to follow very strict specifications when creating a receiver due to the complex environment. The receiver will pick up signals of various strengths in an overcrowded spectrum. Unwanted signals have a negative impact on the communication quality when they are received by the receiver along with a desirable signal.

For the wideband receivers, in most cases, there are out-of-interest bands. The Wi-Fi and GSM bands, for instance, might not be of interest to wideband receivers. Continuous high strength broadcast transmissions in these bands may have an impact on the RF performance of the receiver. In order to prevent blocker signals from being received up by the receiver, bandstop filters are used to attenuate the known blocker signal bands.

These bandstop filters could be used physically or digitally [1]. The use of digital filters may be sufficient to reduce the size of the receiver, but they can only be used after the RF signal has been transformed into the baseband data. As a result, since the blocker has already been processed by the non-linear front-end components, RF performance has already been negatively impacted.

In other situations, different technologies, such as cavity [2], ceramic [3], substrate integrated waveguide (SIW) [4], microstrip [5] could be utilized to realize a physical filter. Cavity filters might not be the best option due to large sizes and mass production times. With the developments in manufacturing technologies, the filters are getting smaller and smaller with ceramic materials. Higher Q values can be reached through ceramic materials, although in some circumstances, such as stripline implementations, lumped elements may not be appropriate. One of the additional implementation techniques is SIW technology. The cross-couplings using SIW technology can be implemented. However, it can be challenging to manufacture the filter by using SIW technology. Besides, this filter may exhibit large insertion losses. On the other hand, the long heritage of microstrip technology and the numerous design options make it a reliable technology.

Different techniques, such as coupled resonators and stubs, could be used to implement microstrip filters. Stub resonators are simple to implement but they have bigger dimensions and more challenging cross-couplings as compared to the other candidate filter. Therefore, stub resonators are not convenient to be used in the compact designs. It is known that

bandstop filters operate effectively with ring resonators [5][6][7][8]. In this architecture, on either side of a through-line, the resonators could be positioned. Coupled resonators radiate power and block signal transmission at the resonant frequencies. In literature [5][6][7][8], there are many studies that the ring resonators have been utilized for designing multi-band filters. However, a few of them are realized through the use of multi-mode resonators [5], while others are realized through the use of various resonators with different resonant frequencies mounted along a through-line [6][7][8].

Dual-mode resonators are typically an effective way to reduce the size of the filter. However, the disadvantage of dual-mode resonators is the degradation of the filter's Q factor [9]. In order to increase the Q factor, a separate resonator is used in a way to resonate at a specific frequency. A typical bandstop response is obtained with two single-mode resonators located along a through line. This is simply the two single-band bandstop filters cascaded upon one another. The length of the through line and the filter increases since it is placed in a cascade configuration. In case the size is an important issue, it may be challenging to implement and place it in a receiver. Furthermore, as the through-line's length is increased, insertion losses increase which is significant at higher frequencies.

In this work, a dual-band bandstop filter is designed and implemented by using SOLR which is a type of ring resonator introduced at [10]. These resonators are placed in a stack configuration. The stack configuration is superior to the cascaded design due to the decreased length of the filter where the length of the dual-band filter is the same as the length of a single-band filter in cascaded configuration [11]. Since the through line's length is reduced by half in stack configuration compared to cascaded configuration, insertion loss is reduced. Through this novel method of stacking SOLR developed in this thesis , two single mode resonators can function as a dual mode resonator. The grouped dual mode resonator has the advantage that just one resonator design is required to achieve dual mode resonance. Additionally, because the resonator's dimensions range between those of a low-frequency and a high-frequency single-mode resonator, it enables low-frequency filters to have comparatively smaller dimensions and high-frequency filters to be manufactured with less difficulty. As a result, a novel way to implement a dual band bandstop filter by using single band bandstop filter coupling matrix is introduced. By using the introduced method, only $(\mathrm{N}+2)\times(\mathrm{N}+2)$ single band coupling matrix is synthesized instead of $(2\mathrm{N}+2)\times(2\mathrm{N}+2)$ dual band coupling matrix. Hence, a compact and less lossy filter is synthesized without giving bigger compromises from the rejection.

To realize the synthesized coupling matrix on the layout, a resonator type should be chosen since this filter synthesis technique is based on multi-resonator structures. These couplings may be self-coupling, which involves coupling within the same resonator, cross coupling, which involves coupling to a resonator that is not directly adjacent. All of these couplings can be utilized by open loop resonators, and by using those couplings, coupling matrices can be implemented. Additionally, the feed points of the first and last resonators must be at least a quarter wavelength apart from each other in order to implement a bandstop filter in a microstrip approach. Open-Loop resonator is a suitable resonator to use since one edge of open-loop resonators is roughly 1/8 of the operating wavelength [10].

In this study, Open-Loop Resonators are simulated by RT/Duroid 6010 substrate with 1.27 mm thickness and 10.7 relative dielectric constant. The high dielectric constant allows for the creation of a small dual-band bandstop filter. Two LTE broadcast bands (2110 MHz–2200 MHz and 2500 MHz–2690 MHz) are covered by the filter's rejection band, which is designed to isolate receivers from interference caused by those frequently used broadcast bands. However, considering the practical aspects of manufacturing cost, designed filter is implemented on an FR-4 substrate. During this transition, the same synthesized coupling matrix is used but the dimensions are recalculated due to the different relative dielectric constant and substrate thickness. Although FR-4 may not offer the same level of performance as RT/Duroid 6010, the filter on FR-4 substrate was manufactured and measured. The performance evaluation of the realized filter is given in the following sections. The following sections describe the outcomes and the design process.

2. SYNTHESIS METHOD OF THE PROPOSED FILTER

In this work, coupled resonator filters are chosen to be implemented. In these filters, resonators have certain coupling coefficients between them to provide required filter response. To find the required coupling coefficients and resonator couplings, coupling matrix (M) must be synthesized.

To synthesize the coupling matrix (M), Chebyshev polynomial has to be synthesized first. This polynomial is used to synthesize the Coupling Matrix of the single band bandpass filter. That coupling matrix is then transformed into a single band bandstop filter. After having single band bandstop filter, grouped single mode resonators are used to have dual mode resonators. As a result of dual mode resonators, dual band response become achievable. Details of the synthesis method are given in the following subsection.

2.1.Chebyshev Polynomial Synthesis

In 1999, R. Cameron introduced a novel method to synthesize a coupling matrix [12] and its Chebyshev function. Chebyshev function provides high selectivity, equi-ripple amplitude characteristics at the in-band, low signal degradation, and high out of band rejection. While synthesizing the Chebyshev function, transmission zeros could be prescribed. With the prescribed transmission zeros, the sharpness of the filter and in-band group delay could be adjusted. These prescribed transmission zeros could be placed symmetrically or asymmetrically. The coupling matrix's dimension minus two might be the maximum number of the placed zeros because at least two transmission zeros must be set at infinity [12].

As a prior step to start the Chebyshev Polynomial synthesis; the fractional bandwidth of the filter, prescribed transmission zeros, and in-band reflection level of the filter should be chosen. First, the functions S_{11} and S_{21}, which represent the desired filter characteristic, are defined by Eq. (2.1) and Eq. (2.2). Here, the fraction of two polynomials $F_N(\omega)$ and $E_N(\omega)$ and $P_N(\omega)/\varepsilon$ and $E_N(\omega)$ are detailed in [12].

$$S_{11}(\omega) = \frac{F_N(\omega)}{E_N(\omega)} \tag{2.1}$$

$$S_{21}(\omega) = \frac{P_N(\omega)}{\varepsilon E_N(\omega)} \tag{2.2}$$

The subscript N represents the degree of the polynomial. All of the polynomials are normalized such that highest degree coefficients of the polynomials are unity. $P_N(\omega)$ is the polynomial that represents the transfer functions' transmission zeros and could be written as in Eq. (2.3).

$$P(\omega) = \prod_{n=1}^{n_{fz}} (\omega - \omega_n) \tag{2.3}$$

In equation (2.3), ω_n is the angular frequency that represents the position of the n th transmission zero.

To have simpler mathematical equations, ω is used as the independent variable of each polynomial which is the amplitude of the complex frequency variable $s = j\omega$. The numerator of the S_{21} in equation (2.4) is normalized by ε to have an equi-ripple response at cutoff frequencies, $\omega = \pm 1$. ε is defined by Eq. (2.4) [13].

$$\varepsilon = \frac{1}{\sqrt{10^{RL/10} - 1}} * \frac{P_N(\omega)}{F_N(\omega)} \text{ , where } \omega = 1 \tag{2.4}$$

From the definition of the Chebyshev function, all reflection zeros are real and placed on the real axis [12]. By using the lossless network alternating pole formula defined by Eq. (2.1) and Eq.(2.2) Eq. (2.5) can easily be defined. ,

$$S_{21}(\omega) * S_{21}(\omega)^* = \frac{P(\omega) * P(\omega)^*}{\varepsilon^2 E(\omega) * E(\omega)^*} \tag{2.5}$$

Right hand side of the equation (2.5) also can be written as in Eq. (2.6) [12]:

$$S_{21}(\omega) * S_{21}(\omega)^* = \frac{1}{\left[1 - j\frac{\varepsilon}{\varepsilon_R} kC_N(\omega)\right] * \left[1 - j\frac{\varepsilon}{\varepsilon_R} kC_N(\omega)^*\right]} \tag{2.6}$$

where,

$$kC_N(\omega) = \frac{F(\omega)}{P(\omega)} \tag{2.7}$$

In Eq. (2.7), k is a constant that normalizes the $C_N(\omega)$. Since the $P_N(\omega)$ and $F_N(\omega)$ are normalized polynomials, k is unity. $C_N(\omega)$ is the Chebyshev filtering function. Which is an N th degree polynomial, and its poles are the roots of $P(\omega)$ and zeros are the roots of $F(\omega)$.

Since k = 1, equation (2.7) can be simplified as in Eq. (2.8).

$$C_N(\omega) = \frac{F(\omega)}{P(\omega)} \tag{2.8}$$

It is known that a General Chebyshev function could be defined by Eq. (2.9) [13]

$$C_N(\omega) = \cosh\left[\sum_{n=1}^{N} \cosh^{-1}(x_n(\omega))\right] \tag{2.9}$$

Since cosh(θ) = cos(jθ), the expression in Eq. (2.9) can alternatively be written as in Eq. (2.10) [13]:

$$C_N(\omega) = \cos\left[\sum_{n=1}^{N} \cos^{-1}(x_n(\omega))\right] \tag{2.10}$$

Equation (2.9) can be used when $|\omega| \geq 1$ and equation (2.10) can be used when $|\omega| < 1$.

Here,

$$x_n = \frac{\omega - \frac{1}{\omega_n}}{1 - \frac{\omega}{\omega_n}} \tag{2.11}$$

In Eq. (2.11) ω_n is the locations of the transmission zeros.

It can easily be seen from Eq. (2.10) that;

- $|\omega| = 1 \Rightarrow C_N = 1$
- $|\omega| < 1 \Rightarrow C_N \leq 1$
- $|\omega| > 1 \Rightarrow C_N > 1$

Hence, C_N complies with all the requirements to be a Chebyshev response. If all of the transmission zeros are placed at infinity, the C_N function could be defined as a pure Chebyshev function as in Eq. (2.12) .

$$C_N(\omega)_{|\omega_n \to \infty} = \cosh\left[N \cosh^{-1}(\omega)\right] \tag{2.12}$$

The following rules should be followed when determining prescribed transmission zeros [12];

- It should be symmetric with respect to the imaginary axis to have purely real coefficients at $C_N(\omega)$ function's numerator and denominator polynomials.
- Number of finite positioned prescribed transmission zeros should be less than or equal to the degree of the $C_N(\omega)$ function which is N.
- If the number of finite positioned prescribed transmission zero counts is less than the degree of the $C_N(\omega)$ function, all the remaining transmission zeros must be placed at infinity.

To realize the Chebyshev function for a two-port canonical network, the maximum number of finite transmission zeros could be N-2. For this reason, minimum two transmissions zeros shall be placed at infinity.

After defining the transmission zeros, the $C_N(\omega)$'s numerator and denominator polynomials coefficients should be determined. After that, by using polynomials, a prototype network with desired $S_{21}(\omega)$ response could be synthesized.

The first step of the polynomial synthesis is to replace $\cosh^{-1}$ with its trigonometric identity [13] as described in Eq. (2.13) and Eq. (2.14);

$$C_N(\omega) = \cosh\left[\sum_{n=1}^{N} \cosh^{-1}(x_n)\right] \tag{2.13}$$

$$\downarrow$$

$$C_N(\omega) = \cosh\left[\sum_{n=1}^{N} \ln(a_n + b_n)\right] \tag{2.14}$$

Here, $a_n = x_n$ and $b_n = (x_n^2 - 1)^{1/2}$. After that, $C_N(\omega)$ can be rewritten as in equation (2.15) by which equation (2.16) can easily be derived [13].

$$C_N(\omega) = \frac{1}{2}\left[\exp\left(\sum \ln(a_n + b_n)\right) + \exp\left(-\sum \ln(a_n + b_n)\right)\right] \tag{2.15}$$

$$C_N(\omega) = \frac{1}{2}\left[\prod_{n=1}^{N}(a_n + b_n) + \frac{1}{\prod_{n=1}^{N}(a_n + b_n)}\right] \tag{2.16}$$

Here, If the second term of the $C_N(\omega)$ given in (2.16) is multiplied by the $\prod_{n=1}^{N}(a_n - b_n)$ and the identity given in (2.17) is used, Eq.(2.16) can be rearranged as in Eq. (2.18).

$$\prod_{n=1}^{N}(a_n + b_n) * \prod_{n=1}^{N}(a_n - b_n) = \prod_{n=1}^{N}(a_n^2 - b_n^2) = 1 \tag{2.17}$$

$$C_N(\omega) = \frac{1}{2}\left[\prod_{n=1}^{N}(a_n + b_n) + \prod_{n=1}^{N}(a_n - b_n)\right] \tag{2.18}$$

After that, to have the final form of the $C_N(\omega)$ given in equation (2.18), $C_N(\omega)$ could be written in terms of c_n and d_n as follows. The details are given in [13];

$$C_N(\omega) = \frac{1}{2}\left[\frac{\prod_{n=1}^{N}(c_n + d_n) + \prod_{n=1}^{N}(c_n - d_n)}{\prod_{n=1}^{N}\left(1 - \frac{\omega}{\omega_n}\right)}\right] \tag{2.19}$$

Where,

$$\begin{aligned} c_n &= \omega - \frac{1}{\omega_n} \\ d_n &= \omega'\left(1 - \frac{1}{\omega_n^2}\right)^2 \\ &= (\omega^2 - 1)^{1/2} \end{aligned} \tag{2.20}$$

Here, ω' is defined as a transformed frequency variable.

Cameron [12] introduced a "recursive technique" to find the coefficients of the $F_N(\omega)$ polynomial, which is the numerator of the $C_N(\omega)$ given in (2.8). After finding the coefficients of the $F_N(\omega)$ polynomial, all other polynomials can be determined. The derivation process is covered in [12]. The Recursive Technique to find the coefficients of $F_N(\omega)$ polynomial is summarized in the following paragraphs.

First, $F_N(\omega)$ has to be written in terms of a new auxiliary function $G_N(\omega)$ as described through Eq. (2.21)-(2.23) .

$$\text{Num}[C_N(\omega)] = F_N(\omega) = \frac{1}{2}[G_N(\omega) + G'_N(\omega)] \tag{2.21}$$

Where,

$$G_N(\omega) = \prod_{n=1}^{N}[c_n + d_n] = \prod_{n=1}^{N}\left[\left(\omega - \frac{1}{\omega_n}\right) + \omega'\left(1 - \frac{1}{\omega_n^2}\right)^{\frac{1}{2}}\right] \tag{2.22}$$

$$G'_N(\omega) = \prod_{n=1}^{N}[c_n - d_n] = \prod_{n=1}^{N}\left[\left(\omega - \frac{1}{\omega_n}\right) - \omega'\left(1 - \frac{1}{\omega_n^2}\right)^{\frac{1}{2}}\right] \quad (2.23)$$

$G_N(\omega)$ in Eq. (2.24) could be written in terms of two auxiliary polynomials which are $U_N(\omega)$ and $V_N(\omega)$. $U_N(\omega)$ is the polynomial that contains the coefficients of only ω variable given in equation (2.25). $V_N(\omega)$ is the multiplication of the $U_N(\omega)$'s coefficients with transformed variable ω' given in equation (2.26).

$$G_N(\omega) = U_N(\omega) + V_N(\omega) \quad (2.24)$$

Where the auxiliary polynomial $U_N(\omega)$ and $V_N(\omega)$ are described by Eq. (2.25) and Eq. (2.26) respectively.

$$U_N(\omega) = u_0 + u_1\omega + u_2\omega^2 + \cdots + u_N\omega^N \quad (2.25)$$

$$V_N(\omega) = \omega'(v_0 + v_1\omega + v_2\omega^2 + \cdots + v_N\omega^N) \quad (2.26)$$

This recursion process is cycling by using the prescribed transmission zeros. At first, the process is initiated by ω_1, which is the first prescribed transmission zero. To calculate $G_1(\omega)$, $V_1(\omega)$ and $U_1(\omega)$ must be calculated as defined by Eq. (2.27). Here, note that auxiliary variables are used.

$$G_1(\omega) = [c_1 + d_1]$$

$$G_1(\omega) = \left(\omega - \frac{1}{\omega_1}\right) - \omega'\left(1 - \frac{1}{\omega_1^2}\right)^{\frac{1}{2}} \quad (2.27)$$

$$G_1(\omega) = U_1(\omega) + V_1(\omega)$$

To calculate the $G_2(\omega)$, $G_1(\omega)$ must be multiplied by ω_2's terms as shown in Eq. (2.28), Eq. (2.29) and Eq. (2.30);

$$G_2(\omega) = G_1(\omega) * [c_2 + d_2] \tag{2.28}$$

$$G_1(\omega) = [U_1(\omega) + V_1(\omega)]\left[\left(\omega - \frac{1}{\omega_2}\right) + \omega'\left(1 - \frac{1}{\omega_2^2}\right)^{\frac{1}{2}}\right] \tag{2.29}$$

$$G_1(\omega) = U_2(\omega) + V_2(\omega) \tag{2.30}$$

After the multiplication, the terms have to be arranged to include only the ω terms to $U_2(\omega)$ and the terms multiplied by ω' to $V_2(\omega)$ as shown in Eq.(2.31) and Eq. (2.32). Also, ω' $V_n(\omega)$ is equal to $(\omega^2 - 1) * (v_0 + v_1\omega + v_2\omega^2 + \cdots + v_n\omega^n)$ and it is in terms of ω. So,

$U_n(\omega)$ could be calculated as Eq. (2.31),

$$U_n(\omega) = \omega U_{n-1}(\omega) - \frac{U_{n-1}(\omega)}{\omega_n} + \left(1 - \frac{1}{\omega_n^2}\right)^{\frac{1}{2}} \omega' V_{n-1}(\omega) \tag{2.31}$$

$$V_n(\omega) = \omega V_{n-1}(\omega) - \frac{V_{n-1}(\omega)}{\omega_n} + \left(1 - \frac{1}{\omega_n^2}\right)^{\frac{1}{2}} \omega' U_{n-1}(\omega) \tag{2.32}$$

This loop shall be used until all of the prescribed transmission zeros are used. With the same process, $G'_N(\omega)$ could be calculated. It can be found that $U'_N(\omega) = U_N(\omega)$ and $V'_N(\omega) = -V_N(\omega)$. Also, $U_N(\omega)$ is equal to the numerator of $F_N(\omega)$ after (N-1) cycles [12]. Since $F_N(\omega)$ is derived by following this method and $P_N(\omega)$ is already known, $E_N(\omega)$ can be determined by using $F_N(\omega)$ and $P_N(\omega)$.

2.2.Coupling Matrix Synthesis

To begin the coupling matrix synthesis process, the scattering matrix elements $S_{11}(s)$ and $S_{21}(s)$ where $s = j\omega$, are defined as follows in Eqs. (2.33)-(2.34) [13] :

$$S_{11}(s) = \frac{F(s)}{E(s)} \tag{2.33}$$

$$S_{21}(s) = \frac{P(s)}{\varepsilon E(s)} \tag{2.34}$$

Here, $E(s)$, $F(s)$ and $P(s)$ are as explained in Section 2.1. Generally, the coefficients of the $E(s)$ polynomial are complex numbers. However, the coefficients of $F(s)$ and $P(s)$ will change with respect to the increasing power of s ($s = j\omega$). The coefficients will change between purely imaginary and purely real. $E(s)$ and $F(s)$ are Nth order polynomials and the $P(s)$'s order is equal to the number of finite prescribed transmission zeros. As mentioned in the Chebyshev polynomial synthesis part (Section 2.1) , minimum two transmission zeros are located at infinity, so $P(s)$'s order should not be more than N-2 [12]. To obtain the coupling matrix, two elements of short circuit admittance parameters y_{21} and y_{22} [14] are to be calculated by using $E(s)$, $F(s)$ and $P(s)$ polynomials.

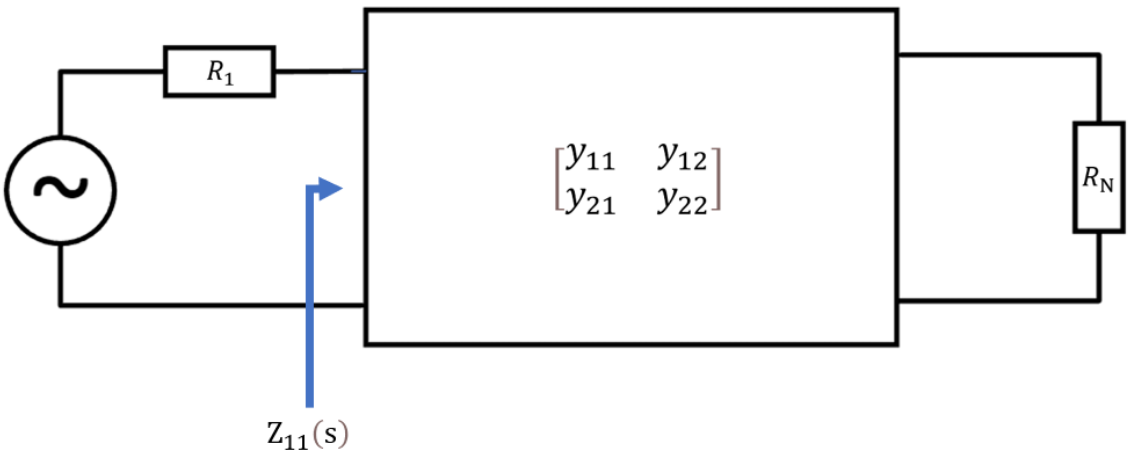

Figure 2.1. Two port circuit with source and load impedances

In Figure 2.1, R_1 is the internal impedance of the voltage source and R_N is the load impedance. Driving point impedance of the whole network including R_N which is denoted by $Z_{11}(s)$, could be found by using open and short circuit parameters as given by Eq. (2.35) [14].

$$Z_{11}(s) = \frac{z_{11}\left[\frac{1}{y_{22}} + R_N\right]}{z_{22} + R_N} \tag{2.35}$$

Since R_N is the normalized load impedance, it equals to one ohm., In case the internal impedance of the voltage source R_1 is also normalized to one ohm, the equation 2.35 can be rewritten as in Eq. (2.36) below.

$$Z_{11}(s) = \frac{z_{11}\left[\frac{1}{y_{22}} + R_N\right]}{z_{22} + R_N} = \frac{z_{11}\left[\frac{1}{y_{22}} + 1\right]}{z_{22} + 1} \tag{2.36}$$

Then, the $Z_{11}(s)$ can be defined by Eq. (2.37) below [12].

$$Z_{11}(s) = \frac{1 - S_{11}(s)}{1 + S_{11}(s)} = \frac{E(s) \pm F(s)}{E(s) \mp F(s)} = \frac{m_1 + n_1}{m_2 + n_2} \tag{2.37}$$

Here, m_1 and m_2 are complex even polynomials and, n_1 and n_2 are complex-odd polynomials [14]. These polynomials are defined in terms of complex variable s and derived from $E(s)$ and $F(s)$.

With an arrangement in the equation (2.37), the numerator of the equation can be rearranged as in Eq. (2.38).

$$Z_{11}(s) = \frac{n_1\left[\frac{m_1}{n_1} + 1\right]}{m_2 + n_2} \tag{2.38}$$

If the equation (2.38) and equation (2.36) are compared, it could be seen that,

$$y_{22} = \frac{n_1}{m_1} \tag{2.39}$$

$$y_{21} = \frac{P(s)/\varepsilon}{m_1} \tag{2.40}$$

Since the denominators of the y_{21} and y_{22} are the same, the transmission zeros of y_{21} and $S_{21}(s)$ will be the same. So, y_{21} can be written eq. (2.40):

If N is an odd number, with the same method in [14], y_{22} and y_{21} can be written as in Eq. (2.41) and Eq. (2.42).

$$y_{22} = \frac{m_1}{n_1} \tag{2.41}$$

and

$$y_{21} = \frac{P(s)}{\varepsilon n_1} \tag{2.42}$$

m_1 and n_1 could be evaluated from $E(s)$ and $F(s)$ by using Eq. (2.37) and Eq. (2.43) [14].

$$m_1 + n_1 = \text{num}[Z_{11}(s)] = E(s) + F(s) \tag{2.43}$$

Then auxiliary functions $m_1(s)$ and $n_1(s)$ can be written as below [14] .

$$m_1(s) = \text{Re}(e_0 + f_0) + j * \text{Im}(e_1 + f_1)s + \text{Re}(e_2 + f_2)s^2 + \cdots \tag{2.44}$$

And

$$n_1(s) = j * \text{Im}(e_0 + f_0) + \text{Re}(e_1 + f_1)s + j * \text{Im}(e_2 + f_2)s^2 + \cdots \tag{2.45}$$

Here, e_i and f_i are the coefficients of the $E(s)$ and $F(s)$ polynomials. With this procedure defined in [14], m_1 and m_2 has purely real coefficients because, here the highest

degree terms of the $E(s)$ and $F(s)$ are purely real and $P(s)$'s degree is smaller than N. Also y_{21} and y_{22}'s common denominator is an N th degree polynomial and their numerators' degree is smaller than N. These terms could be summarized as defined in Eq. (2.46) to (2.51).

If N is even , $y_{21}(s)$ and $y_{22}(s)$ can be defined by Eq. (2.46) and Eq. (2.47).

$$y_{21}(s) = \frac{y_{21n}(s)}{y_d(s)} = \frac{\frac{P(s)}{\varepsilon}}{m_1(s)} \tag{2.46}$$

$$y_{22}(s) = \frac{y_{22n}(s)}{y_d(s)} = \frac{n_1(s)}{m_1(s)} \tag{2.47}$$

If N is odd , $y_{21}(s)$ and $y_{22}(s)$ becomes as defined by Eq. (2.48) and Eq. (2.49) [14].

$$y_{21}(s) = \frac{y_{21n}(s)}{y_d(s)} = \frac{\frac{P(s)}{\varepsilon}}{n_1(s)} \tag{2.48}$$

$$y_{22}(s) = \frac{y_{22n}(s)}{y_d(s)} = \frac{m_1(s)}{n_1(s)} \tag{2.49}$$

Where the auxiliary polynomials $m_1(s)$ and $n_1(s)$ are given below.

$$m_1(s) = Re(e_0 + f_0) + j * Im(e_1 + f_1)s + Re(e_2 + f_2)s^2 + \cdots \tag{2.50}$$

$$n_1(s) = j * Im(e_0 + f_0) + Re(e_1 + f_1)s + j * Im(e_2 + f_2)s^2 + \cdots \tag{2.51}$$

By using equations (2.50) and (2.51) ; auxiliary polynomials $m_1(s)$ and $n_1(s)$ can be calculated in terms of e_i and f_i, which are the coefficients of $E(s)$ and $F(s)$. Since the numerator and denominator polynomials belonging to $y_{21}(s)$ and $y_{22}(s)$ are obtained, their

residues could be evaluated by using partial fraction expansion method. The eigenvalues of $y_d(s)$ are common with $y_{21}(s)$ and $y_{22}(s)$. $y_d(s)$ is a N th degree polynomial, and its roots are purely imaginary. Then, admittance matrix could be written as below [14].

$$[Y_N] = \begin{bmatrix} y_{11}(s) & y_{12}(s) \\ y_{21}(s) & y_{22}(s) \end{bmatrix} = \frac{1}{y_d(s)} \begin{bmatrix} y_{11n}(s) & y_{12n}(s) \\ y_{21n}(s) & y_{22n}(s) \end{bmatrix} \tag{2.52}$$

$$[Y_N] = j \begin{bmatrix} 0 & K_\infty \\ K_\infty & 0 \end{bmatrix} + \sum_{k=1}^{N} \frac{1}{(s - j\lambda_k)} * \begin{bmatrix} r_{11k} & r_{12k} \\ r_{21k} & r_{22k} \end{bmatrix} \tag{2.53}$$

Here K_∞ is zero unless the case is not fully canonical. The number of the prescribed finite transmission zeros is N for canonical case. For canonical case, the numerator of $y_{21}(s)$'s degree is the same as the degree of $y_d(s)$. K_∞ can be calculated from $y_{21}(s)$by reducing the degree of $y_{21}(s)$'s numerator polynomial $y_{21n}(s)$ by one. Then, the residues r_{21k} could be evaluated. Since it is the fully canonical, the number of transmission zeros that are finite (n_{fz}) are equal to N. Since the result of $N - n_{fz} = 0$ is even, $P(s)$ must be multiplied by j to satisfy the unitary conditions stated in [14]. For odd case, this multiplication is not necessary as shown in Eq. (2.55).

$$jK_\infty = \left. \frac{y_{21n}(s)}{y_d} \right|_{s=j\infty} \tag{2.54}$$

$$jK_\infty = \begin{cases} \left. \dfrac{jP(s)/\varepsilon}{y_d} \right|_{s=j\infty}, & N - n_{fz} \text{ is even} \\ \left. \dfrac{P(s)/\varepsilon}{y_d} \right|_{s=j\infty}, & N - n_{fz} \text{ is odd} \end{cases} \tag{2.55}$$

As a result of the y_d calculation process, the coefficient of the highest degree term of the y_d is $1 + 1/\varepsilon_R$. Also, the coefficient of the highest degree term of $P(s)$ is 1. Then K_∞ can be determined by Eq. (2.55) [14],

$$K_\infty = \frac{1}{\varepsilon} * \frac{1}{1 + \frac{1}{\varepsilon_R}} = \frac{\varepsilon_R}{\varepsilon} * \frac{1}{\varepsilon_R + 1} \tag{2.56}$$

Where,

$$\varepsilon_R = \frac{\varepsilon}{\sqrt{\varepsilon^2 - 1}} \tag{2.57}$$

Then, K_∞ could be derived as,

$$K_\infty = \frac{\varepsilon}{\varepsilon_R}(\varepsilon_R - 1) \tag{2.58}$$

And the new numerator polynomial could be written as below and its degree is N – 1,

$$y'_{21n}(s) = y_{21n}(s) - jK_\infty - y_d(s) \tag{2.59}$$

After that, the residues of $y'_{21}(s) = y'_{21n}(s)/y_d(s)$ could be found [14].

Now, by using Eq. (2.60),

$$\begin{aligned}[Y_N] &= \begin{bmatrix} y_{11}(s) & y_{12}(s) \\ y_{21}(s) & y_{22}(s) \end{bmatrix} = \frac{1}{y_d(s)} \begin{bmatrix} y_{11n}(s) & y_{12n}(s) \\ y_{21n}(s) & y_{22n}(s) \end{bmatrix} \\ &= j \begin{bmatrix} 0 & K_\infty \\ K_\infty & 0 \end{bmatrix} + \sum_{k=1}^{N} \frac{1}{(s - j\lambda_k)} * \begin{bmatrix} r_{11k} & r_{12k} \\ r_{21k} & r_{22k} \end{bmatrix} \end{aligned} \tag{2.60}$$

And (2.61),

$$\begin{aligned}[Y_N] &= \begin{bmatrix} y_{11}(s) & y_{12}(s) \\ y_{21}(s) & y_{22}(s) \end{bmatrix} = [y_{SL}] + \sum_{k=1}^{N} \begin{bmatrix} y_{11n}(s) & y_{12n}(s) \\ y_{21n}(s) & y_{22n}(s) \end{bmatrix} \\ &= j \begin{bmatrix} 0 & M_{SL} \\ M_{SL} & 0 \end{bmatrix} + \sum_{k=1}^{N} \frac{1}{(sC_k + jB_k)} \begin{bmatrix} M_{sk}^2 & M_{Sk}M_{Lk} \\ M_{Sk}M_{Lk} & M_{Lk}^2 \end{bmatrix} \end{aligned} \tag{2.61}$$

Comparing Eq. (2.60) and Eq. (2.61), It may be seen that $M_{SL} = K_{\infty}$. Here, k is the resonator number, M_{mn} is the coupling matrix **M**, C and B are the capacitances and susceptances as shown in Figure 2.2. Also, in (2.60) $K_{\infty} = 0$ unless the case is not fully canonical [14].

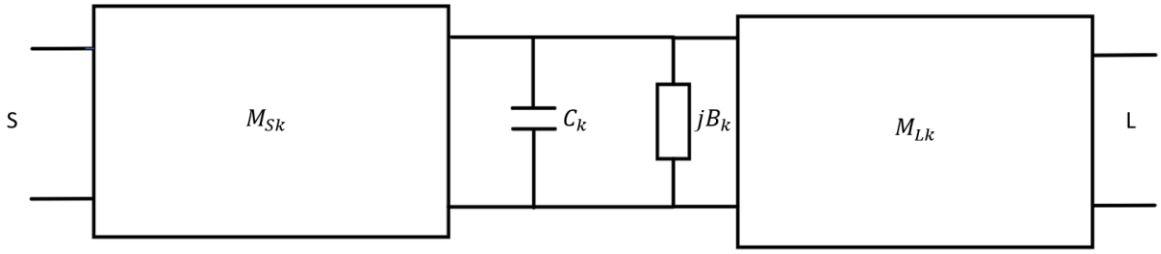

Figure 2.2. Coupling between source kth resonator and load

Here,

$$\frac{r_{21k}}{s - j\lambda_k} = \frac{M_{Sk}M_{Lk}}{sC_k + jB_k} \tag{2.62}$$

$$\frac{r_{22k}}{s - j\lambda_k} = \frac{M_{Lk}^2}{sC_k + jB_k} \tag{2.63}$$

Where the r_{21k} and r_{22k} are the residues and λ_k represents the eigenvalues of S_{21} and S_{22} polynomials [12]. The circuit parameters could be evaluated by equating the real and imaginary parts at the equation (2.62) and (2.63) as below [14].

$$C_k = 1,$$

$$B_k(\equiv M_{kk}) = -\lambda_k,$$

$$M_{Lk}^2 = r_{22k},$$

$$M_{Sk}M_{Lk} = r_{21k},$$

$$M_{Lk} = \sqrt{r_{22k}} = T_{Nk} ,$$

$$\text{and } M_{Sk} = \frac{r_{21k}}{\sqrt{r_{22k}}} = T_{1k}, \; k = 1,2,3, \dots, N \tag{2.64}$$

Here, T which is given in Eq. (2.65) is an $N \times N$ matrix. Each row in matrix T is an orthogonal vector. M_{kk} shows the self couplings, M_{Sk} is the input couplings and the M_{Lk} is the output couplings [12].

$$\mathbf{M} = \begin{bmatrix} M_{SS} & M_{S1} & \cdots & M_{Sk} & \cdots & M_{S,N-1} & M_{SN} & M_{SL} \\ M_{1S} & M_{11} & & & & & & M_{1L} \\ \vdots & & \ddots & & & & & \vdots \\ M_{kS} & & & M_{kk} & & & & M_{kL} \\ \vdots & & & & \ddots & & & \vdots \\ M_{N-1,S} & & & & & M_{N-1,N-1} & & M_{N-1,L} \\ M_{NS} & & & & & & M_{NN} & M_{NL} \\ M_{LS} & M_{L1} & \cdots & M_{Lk} & \cdots & M_{L,N-1} & M_{LN} & M_{LL} \end{bmatrix} \quad (2.65)$$

Once each element of the transversal coupling matrix is determined, the matrix then can be converted to a folded form without affecting the characteristics of the filter. In transversal mode, the coupling matrix has all couplings between all resonators. This is difficult to realize with physical resonators. As a result of that, a conversion is needed to form that matrix into a realizable form. There are several forms for easier implementation like folded canonical, cul-de-sac [15]. In this work, folded canonical form is used to achieve optimized coupling matrix. After establishing a folding algorithm on the coupling matrix, since the aim is to achieve band reject filter, coupling matrix must be converted to change the characteristics from band pass to band stop.

2.3.Bandpass – Bandstop Conversion of the Coupling Matrix

There are several ways to synthesize a bandstop coupling matrix. The, first one is to change the $P(s)$ and $F(s)$ polynomials while synthesizing the coupling matrix [15]. Another option is to synthesize a bandstop coupling matrix. After synthesizing the bandpass coupling matrix (**M**), bandstop coupling matrix could be achieved by taking the inverse of the synthesized bandpass coupling matrix (**M**) [16]. After that operation, the coupling between the resonators would be changed but for the filter response point of view, only the S_{21} and S_{11} responses will change. After these conversions, transmission zero placements will be the same, but transmission zeros are going to be renamed as reflection zeros because they are being carried by S_{11} now. Also, a unity coupling between the source and the load is going to be observed. As a result of that coupling, layout implementation options will be decreased.

$$\mathbf{M}_{\text{BandStop}} = \mathbf{M}_{\text{BandPass}}^{-1} \tag{2.66}$$

2.4.Folding the Coupling Matrix

While folding the coupling matrix, a useful final coupling between the resonators should be aimed. In that way, a common way to fold the coupling matrix is into cul-de-sac form. It provides cross couplings between source and load, also first and last resonator aside the regular adjacent resonator couplings. Figure 2.3 and Figure 2.4 shows the connection schemes between the coupled resonators, those schemes are generated by using the synthesized coupling matrix[15].

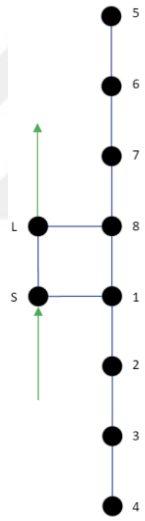

Figure 2.3. 8th degree bandstop filter in Cul-de-Sac configuration [15]

As seen in Figure 2.3., other resonators are connected to first and last resonators in a chained way. Only the first and last resonators are connected to the through line.

A novel way to optimize these couplings without affecting the filter response is proposed (Figure 2.4) by Z.N. He [17].

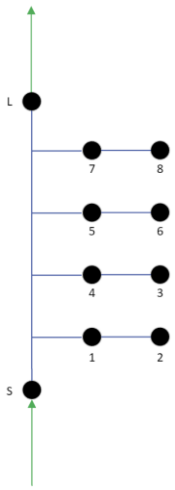

Figure 2.4. 8th degree filter in proposed configuration in [17]

In this work, improved coupling scheme [17] shown in Figure 2.4. is used for the implementation of the layout. In this layout half of the resonators are directly coupled along the through feed line.

2.5.Realization of the Filter Using Coupling Matrix

To realize the coupling matrix as a cross coupled resonator filter, the resonators should be chosen. As mentioned before, the selectivity is one of the most important parameter for filters. To get high selectivity performance, the designer may take an advantage of cross coupled resonators. Cross couplings are the coupling that is not between the adjacent resonators [18]. This alternative path for EM wave provides transmission zeros and with transmission zeros, high selectivity filter could be realized. Generally, those cross couplings are realized by dielectric resonators or cavity filters [15]. There is an alternative method for implementing the cross coupled resonators in microstrip technology. Although, there is one difficulty for the cross couplings in microstrip technology, it is not easy to calculate or adjust the required couplings for cross coupled resonators. Ring resonators are one of the resonator that allows the cross coupling between the resonators and could be implemented in microstrip [10]. In this work, the Square Open-Loop Resonators are chosen as the resonator, which is a type of ring resonator.

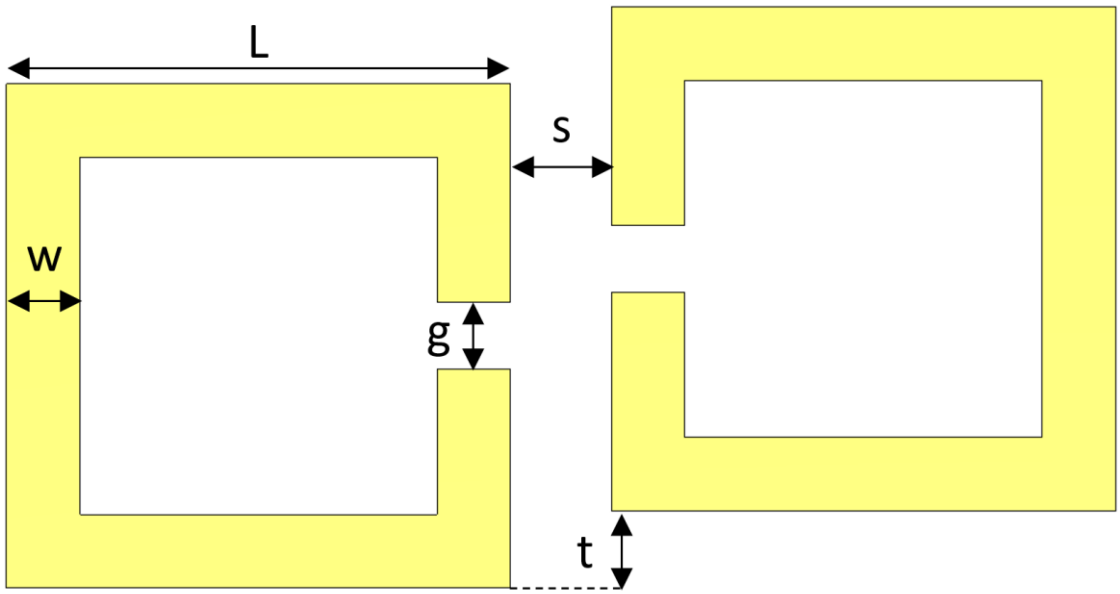

Figure 2.5 Electrically coupled open-loop resonators and design parameters

On Figure 2.5, the electric coupling of two Open-Loop resonators is shown.

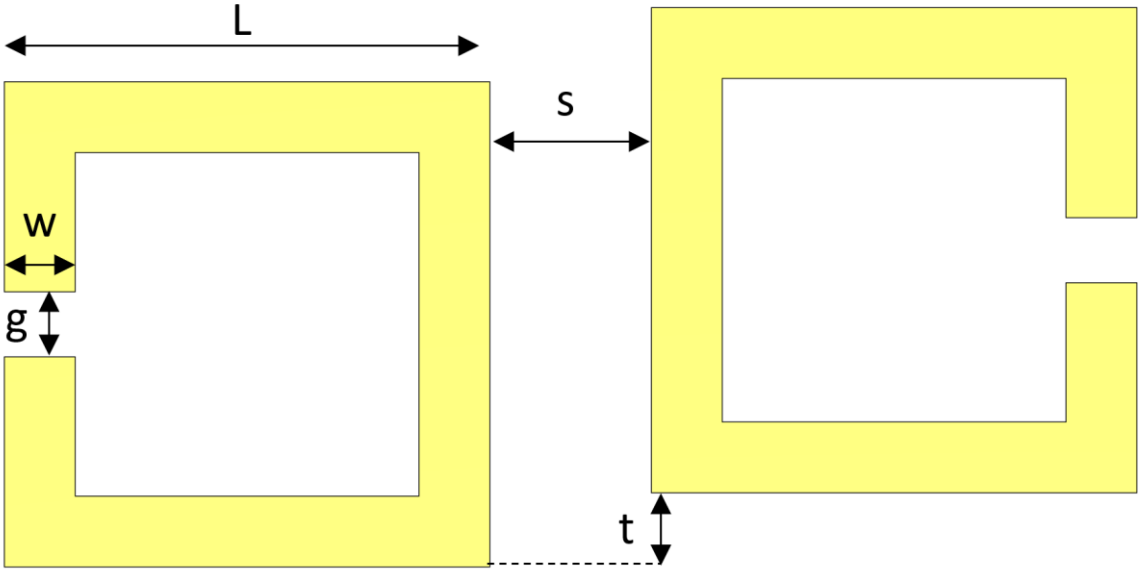

Figure 2.6 Magnetically coupled open-loop resonators and design parameters

On Figure 2.6, the magnetic coupling of two Open-Loop resonators is shown.

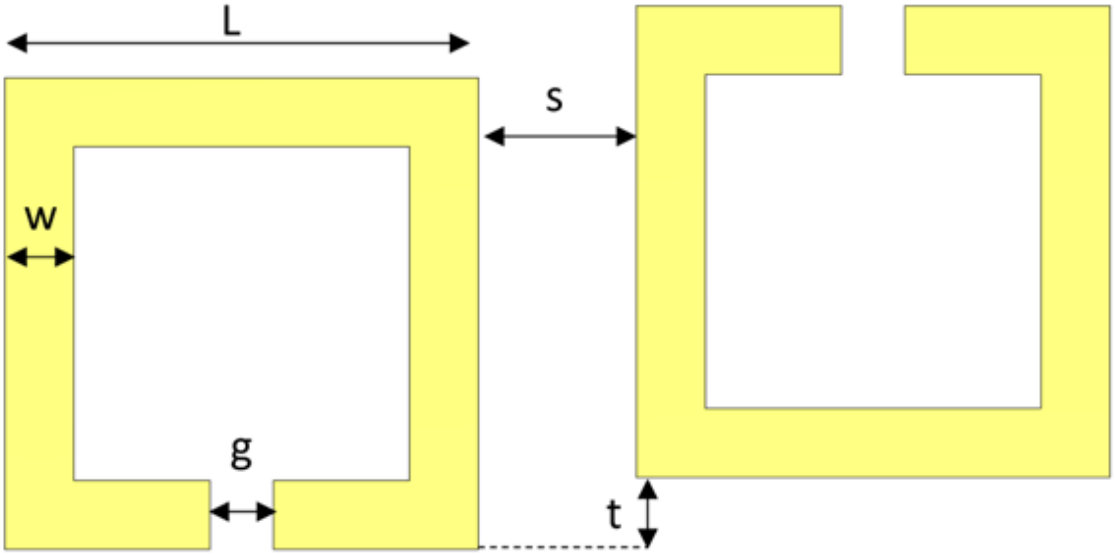

Figure 2.7. Mixed coupled open-loop resonators and design parameters

On Figure 2.7, the mixed coupling of two Open-Loop resonators is shown.

First configuration in Figure 2.5 is used for electrical coupling, second configuration in Figure 2.6 is used for magnetic coupling and the last configuration in figure Figure 2.7 stands for mixed coupling. To calculate the coupling coefficients (k) between the resonators, 3D EM full wave simulation is used. In the s-parameter simulations two peak frequencies could easily observed.

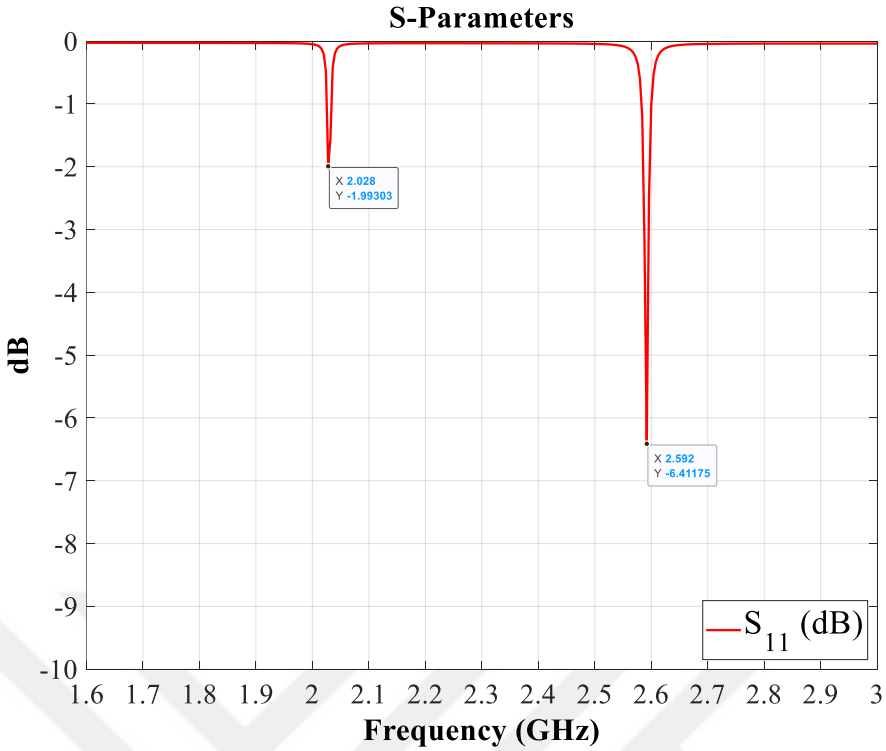

Figure 2.8. Electrical coupling when the distance is 1.25mm

Figure 2.8 shows the electrical coupling, when the distance between two coupled open-loop resonators is 1.25 mm. To see the change on frequencies with respect to the distance between the resonators, different distance is set and simulated again.

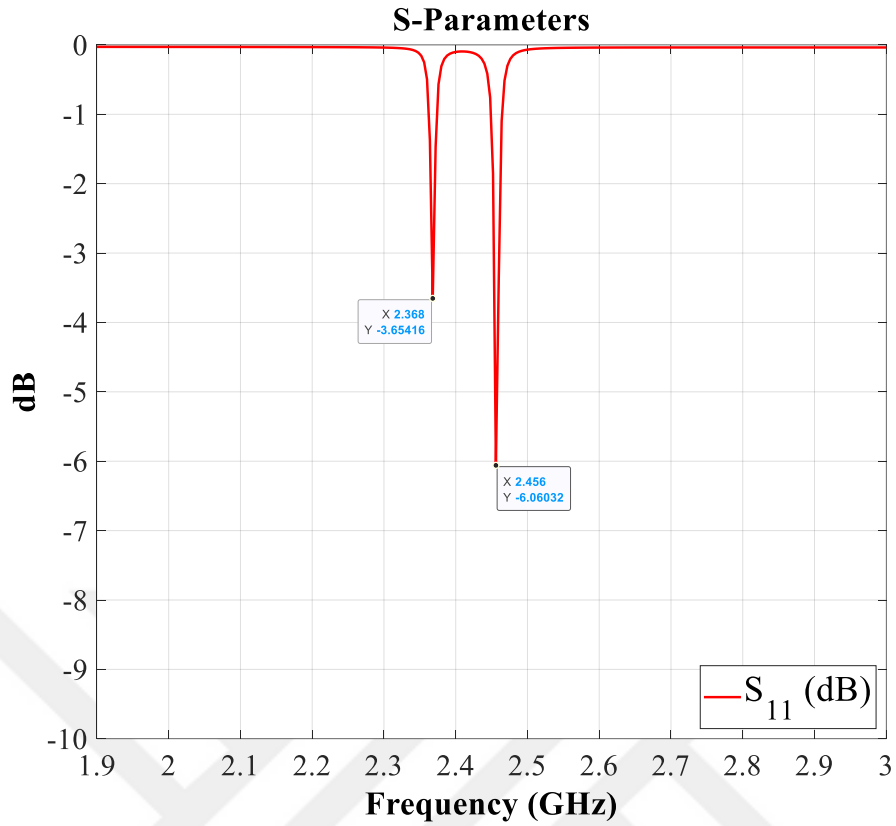

Figure 2.9. Electrical coupling when distance is 2mm

Figure 2.9 shows the electrical coupling, when the distance between two coupled open-loop resonators is 2 mm. As seen, the resonant frequencies are changed, so, the physical coupling coefficient is changed between those two resonators.

The coupling coefficients, k_E (electric), k_M (magnetic) and k_x (mixed) coupling between the two resonators can be calculated as given below [10],

$$k_E = \frac{f_m^2 - f_e^2}{f_m^2 + f_e^2} \quad k_M = \frac{f_e^2 - f_m^2}{f_m^2 + f_e^2} \quad k_X = \frac{f_e^2 - f_m^2}{f_m^2 + f_e^2} \tag{2.67}$$

In (2.67), f_m and f_e are the resonant frequencies when two resonators coupled to each other [10]. These coupling coefficients could be adjusted by changing L, w, s, t and g dimensions of the resonators in Figure 2.5, Figure 2.6 and Figure 2.7.

The relation between the elements of **M** and **k** matrices is as given below [18],

$$\mathbf{M}_{ij} = \frac{f_0}{BW} * \mathbf{k}_{ij} \tag{2.68}$$

This method is only used for calculation of the physical coupling between the resonators. A different method should be used for calculation of the physical coupling between Source/Load and the resonators [18].

It is important to comply the source and load couplings between the ports and the resonators.

There are two different feed techniques for the Square Open-Loop Resonators [19] as below.

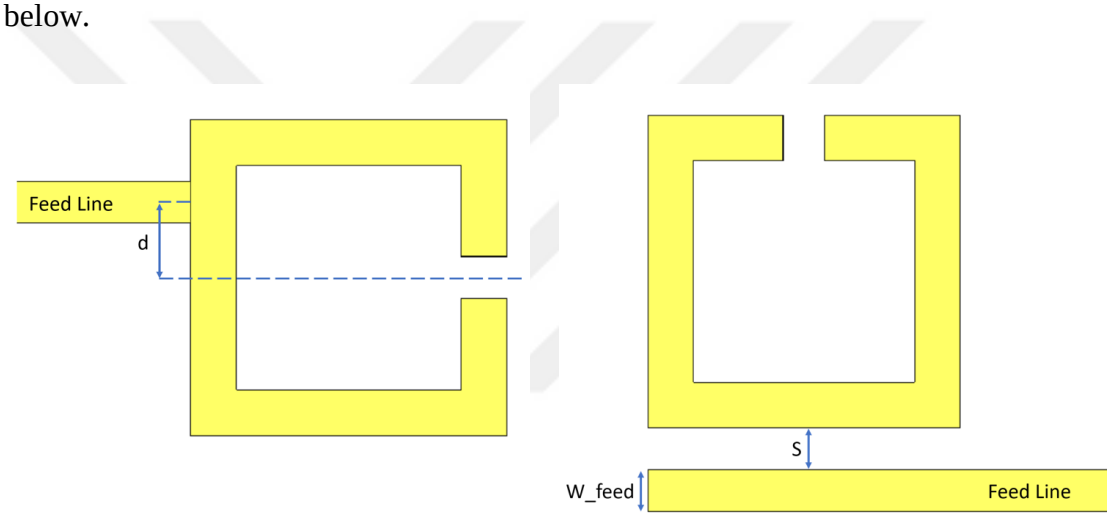

(a) (b)

Figure 2.10. (a) Tapped line fed open-loop resonator. (b) Coupled line fed open-loop resonator

The first technique in Figure 2.10a is the tapped-line feeding method [19]. The feed line has an offset from the middle of the one edge of the resonator. The coupling coefficient will be increased while d is increasing and vice versa. In some cases, for this method the feed line may be tapped in a tapered way to decrease the mismatch losses. The second feeding method in Figure 2.10b is the coupled-line coupling [19]. With this method decreasing the w and/or S, higher coupling coefficient values could be achievable.

Required input and output coupling external quality could be calculated by using equation (2.69). In this equation, Q_e is the external quality factor of the filter's source and load couplings. External quality is the ratio between stored energy on the feed line and

transferred energy to the coupled resonator. It is related with fractional bandwidth of the desired filter and coupling coefficient between the feed and the resonator M_{S1}.

$$Q_e = \frac{1}{FBW * M_{S1}^2} \tag{2.69}$$

Q_e of the designed filter could be calculated in two ways, first one is to use Eigenmode solver on CST Studio Suite [20], it gives the resonance frequencies and Q_e values at that frequency. The other way is to use frequency or time domain solver to have S_{11} response of the single resonator to calculate group delay. After having that group delay response, Q_e of the resonator could be calculated by using equation (2.70) [19] given below

$$Q_e = \frac{2\pi f_0 \cdot \tau(f_0)}{4} \tag{2.70}$$

As seen in equation (2.71), group delay response of the coupling at resonant frequency $\tau(f_0)$ is required. Group delay is a function that gives the delay between the input and output across the frequency and could be calculated by using equation (2.71).

$$\tau(f_0) = -\frac{\Delta\varphi}{\Delta 2\pi f_0} \tag{2.71}$$

After required Q_e and the coupling matrix is calculated. Filter could be realized by using chosen resonators.

Another important parameter for the filter is Unloaded-Q. It is not mandatory to calculate while implementing the filter, but it gives a clue about the loss of the filter [21]. It is the ratio between the stored energy and lost energy on a resonator. High unloaded- Q provides low insertion loss in passband and high rejections at stopband. To calculate unloaded-Q, the effect of the feed line must be removed, else the result of the equation (2.72) below gives loaded-Q instead of unloaded-Q [21].

$$Q_L = \omega_0 \frac{W_{stored}}{P_{loss}} \tag{2.72}$$

The relation between loaded-Q and unloaded-Q is given in equation (2.73). As seen, physical coupling (k) must be calculated to have unloaded-Q value [21].

$$Q_u = Q_L(1 + k) \tag{2.73}$$

Q_u : Unloaded Quality Factor

Q_L : Loaded Quality Factor

k : Input Coupling Coefficient

To calculate k, the coupling ratio of the resonator should be determined to investigate whether it is over coupled or under coupled. This could be seen by observing the S_{11} plot (Figure 2.11) on smith chart graph. If the diameter of the resonator's Q circle (d) is smaller than the radius of the smith chart (r), it is defined as under coupling, else, it is defined as over coupling [21].

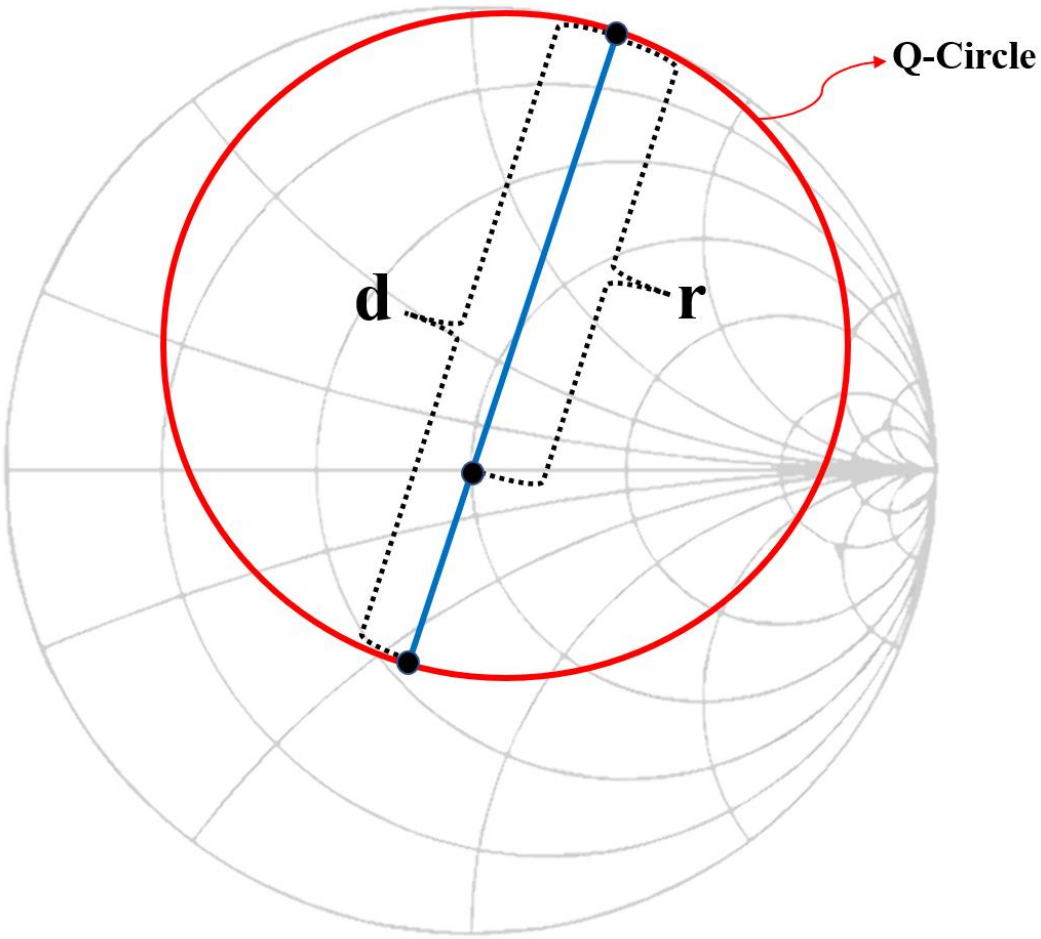

Figure 2.11. Q-Circle on Smith Chart

d： Diameter of Resonator Q Circle

$$k = \frac{d}{2-d} \begin{cases} \text{under coupling } (k < 1) \\ \text{over coupling } (k > 1) \end{cases} \tag{2.74}$$

As a result of coupling, appropriate formula of the k coefficient should be used accordingly [21].

$$k = \frac{1 - 10^{\frac{S_{11}^{min}}{20}}}{1 + 10^{\frac{S_{11}^{min}}{20}}} \quad \{k < 1 \text{ (if resonator is undercoupled)} \tag{2.75}$$

$$k = \frac{1 + 10^{\frac{S_{11}^{min}}{20}}}{1 - 10^{\frac{S_{11}^{min}}{20}}} \quad \{k > 1 \text{ (if resonator is overcoupled)} \tag{2.76}$$

Also loaded-Q is needed to calculate unloaded-Q. To calculate loaded-Q from the S_{11} graph of the resonator, the frequency of the minimum point on the graph should be found. After that, two frequencies must be found that which has $\mp 45°$ degree phase difference with respect to that frequency ($S_{11}^{\emptyset}$, $\phi = \mp 45°$). Since all required three frequencies are found, loaded-Q could be calculated by using equation (2.78).

$$S_{11}^{\emptyset} = 10 \log \frac{1 + 10^{\frac{S_{11}^{min}}{10}}}{2} \tag{2.77}$$

$$Q_L = \frac{f_L}{f_2 - f_1} \tag{2.78}$$

Here, f_L is the frequency of the minimum point of S_{11} graph. f_2 and f_1 are the frequencies that have 45 degrees phase difference with f_L.

Also unloaded-Q could be calculated by using EM simulation tools such as CST Studio Suite. CST Studio Suite has unloaded-Q calculator inside that makes the calculations above with a post processing script.

3. SYNTHESIS AND DESIGN OF THE PROPOSED FILTER

For this work, the objective is to design and implement a dual-band bandstop filter to reject the signals between 2110 MHz – 2200 MHz and 2500 MHz – 2690 MHz bands. The selected substrate material for the open loop resonators is Rogers RT/Duroid 6010 substrate with 1.27 mm thickness.

To start designing filter, a synthesized coupling matrix is needed. As an input to coupling matrix synthesis process, desired frequency band, filter order, desired reflection zero locations are needed. For this work, no prescribed transmission zeros are used. As a result of this, $P_N(\omega)$ equals to unity. Since there are no prescribed zeros are defined for bandpass coupling matrix, there will be no reflection zeros at bandstop coupling matrix after conversion.

$$S_{11}(\omega) = \frac{F_N(\omega)}{E_N(\omega)} \tag{3.1}$$

$$S_{21}(\omega) = \frac{P_N(\omega)}{\varepsilon E_N(\omega)} \tag{3.2}$$

To synthesize and optimize the coupling matrix, SynMatrix [22] coupling matrix synthesis tool is used. SynMatrix is a software that takes the required filter parameters and solves these polynomials. Final optimized coupling matrix is shown below.

$$\mathbf{M} = \begin{bmatrix} 0 & 2.024 & 0 & 1 \\ 2.024 & 0 & 0.0001 & 0 \\ 0 & 0.0001 & 0 & 2.024 \\ 1 & 0 & 2.024 & 0 \end{bmatrix} \tag{3.3}$$

After optimization, $\mathbf{M}_{12}$ is almost taken as zero to achieve the desired result.

To realize the filter open loop resonators are used. To have a dual band response, two single mode open loop resonators are used as a combined dual mode resonator. Resonant frequencies and Q_e values are simulated by using CST Studio Suite 2021. One resonator and a feed line are simulated as shown in Figure 3.5 to see the resonance frequency of a

single resonator by using Eigenmode solver in CST. Eigenmode solver is shown in Figure 3.1.

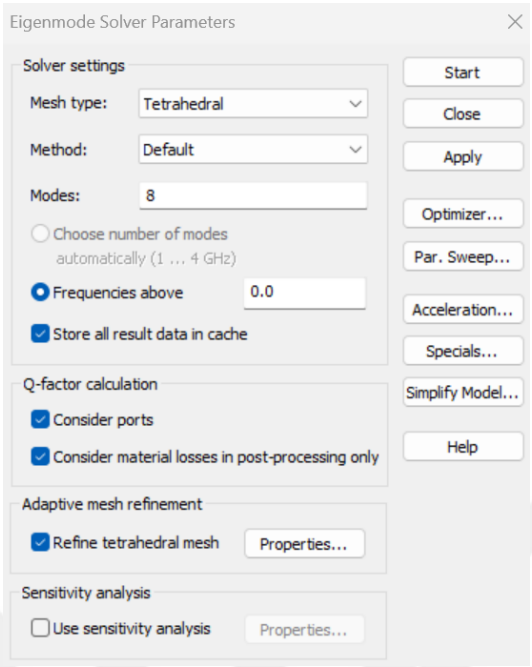

Figure 3.1. Eigenmode solver parameters

To see the resonance frequencies and external Q values "Consider Ports" check box should be selected. Also, number of modes is set up to 8 to check any undesired resonance modes up to 8th mode.

Also, boundary conditions are set to electric wall on each side to run Eigenmode Solver as seen in Figure 3.2. Electric wall distance for Z_{max} is taken as the height of the waveguide port on the simulation. This height is calculated by using port extension coefficient macro on CST Studio Suite 2021. As a thumb rule, it shouldn't be less than 5 times of the substrate height.

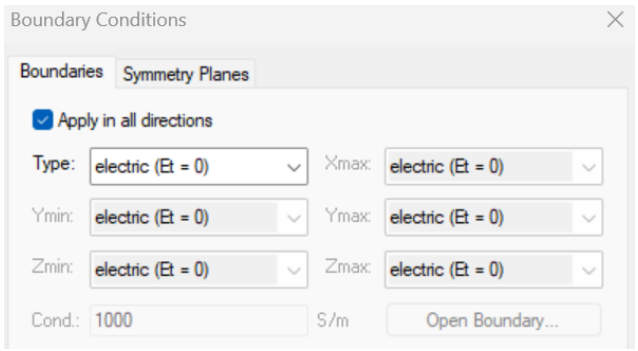

Figure 3.2. Boundary Conditions that is used on external-Q simulations

Electric wall boundary box is shown in Figure 3.3.

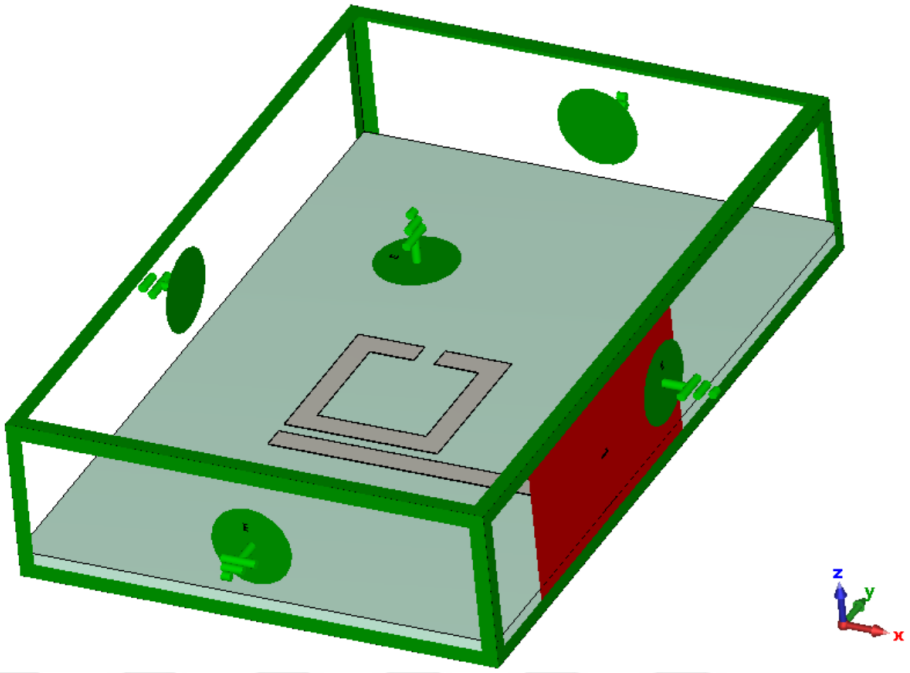

Figure 3.3. Bounding Box that is used on external-Q simulations

Dimensions of the single resonator is shown in Figure 3.4. Width of the open loop resonator is 50 Ω at filter center frequency and the electrical length of the resonator is equal to 90° at the same frequency.

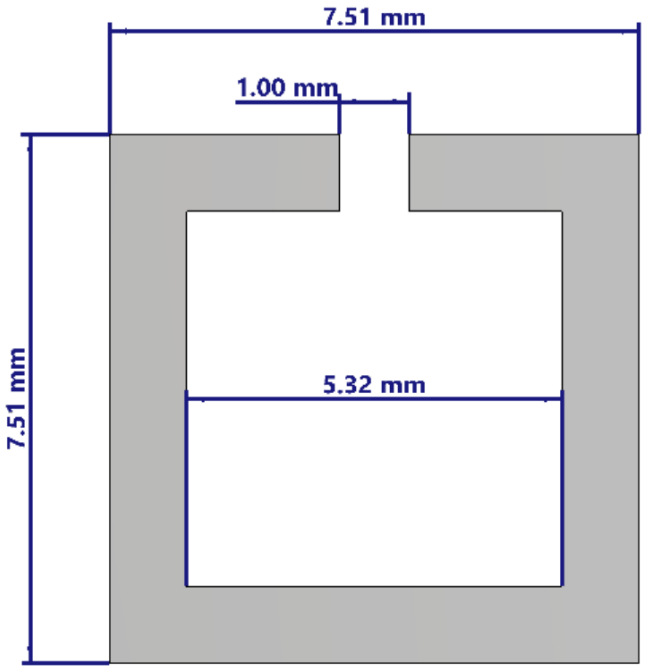

Figure 3.4. Designed Open-loop resonator

Resonator are excited by using coupled line feed method as seen in Figure 3.5. Waveguide port is used in Quasi-TEM mode to excite microstrip feed.

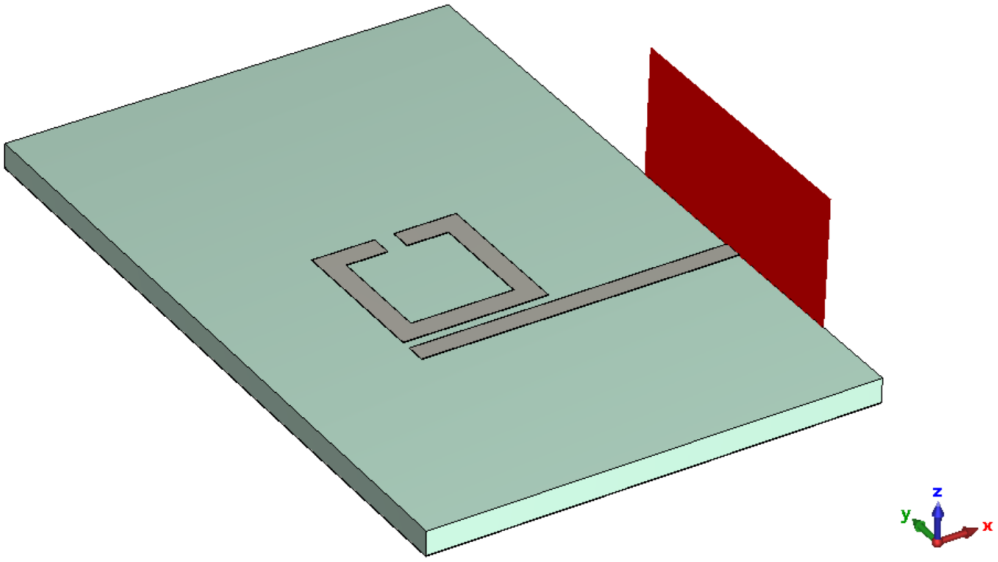

Figure 3.5. Coupled line excitation

E-Field lines around the microstrip line cross section can be seen in Figure 3.6. Hence the excited propagation mode is Quasi-TEM for microstip traces, there is no symmetry on x-axis because there is no ground above the microstrip trace.

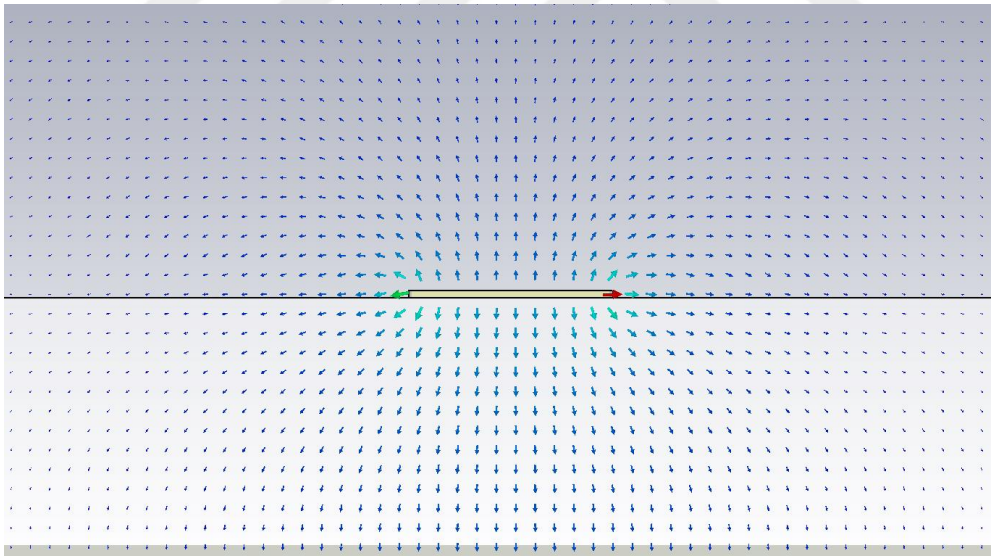

Figure 3.6. E-Field on the Cross-Sectional area of the microstrip feed line

As shown in Figure 3.7, first mode of the resonator is at 2.395 GHz and the next mode is at 4 GHz. This first resonant frequency is the geometrically mean of the desired dual band's center frequencies.

External Q-factor results:

Mode	Loaded Frequency	External Q
3	2.395 GHz	88.33
4	4 GHz	0.8209

Figure 3.7. Single mode resonator external Q simulation results on CST

To have a dual mode resonator, another single mode resonator coupled to the resonator as shown in Figure 3.8 below.

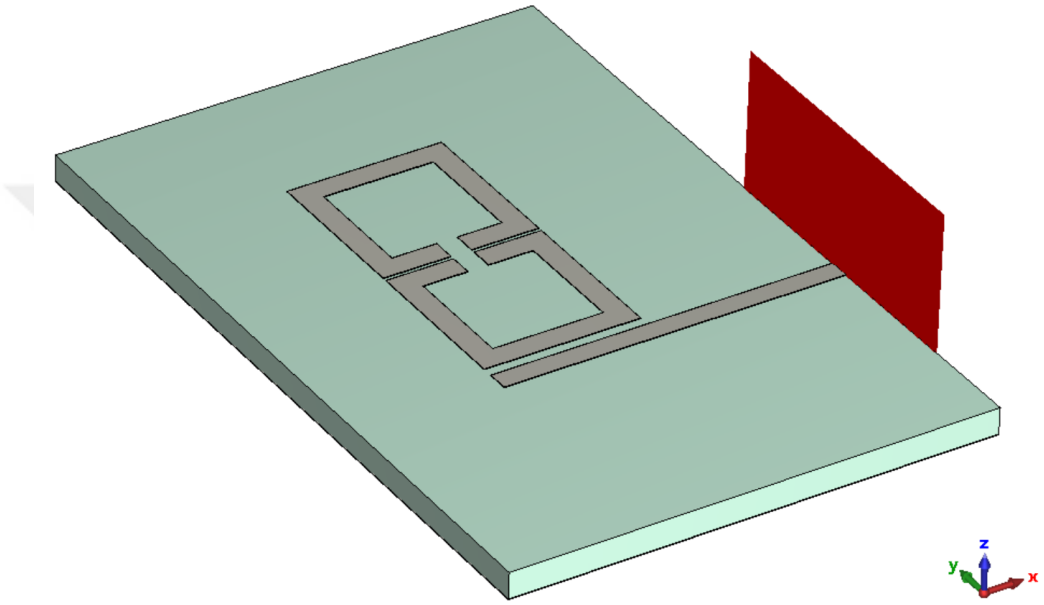

Figure 3.8. Excitation of dual mode resonator with coupled line feed

External Q-factor computation completed.

External Q-factor results:

Mode	Loaded Frequency	External Q
4	2.165 GHz	262
5	2.59 GHz	147

Figure 3.9. Dual mode resonator external Q simulation results on CST

As a result of this dual mode resonator simulation geometrical mean of first two resonant frequencies are calculated as below,

$$f_{c_{dualband}} = \sqrt[2]{f_{c_{first\ band}} * f_{c_{second\ band}}} = \sqrt[2]{2.165 * 2.59} = 2.36 \cong 2.395 \quad (3.4)$$

For the first mode at 2.165 GHz E-Field can be seen in Figure 3.10. For this mode, as seen, the electric field density has its peak values on the area that between the resonators.

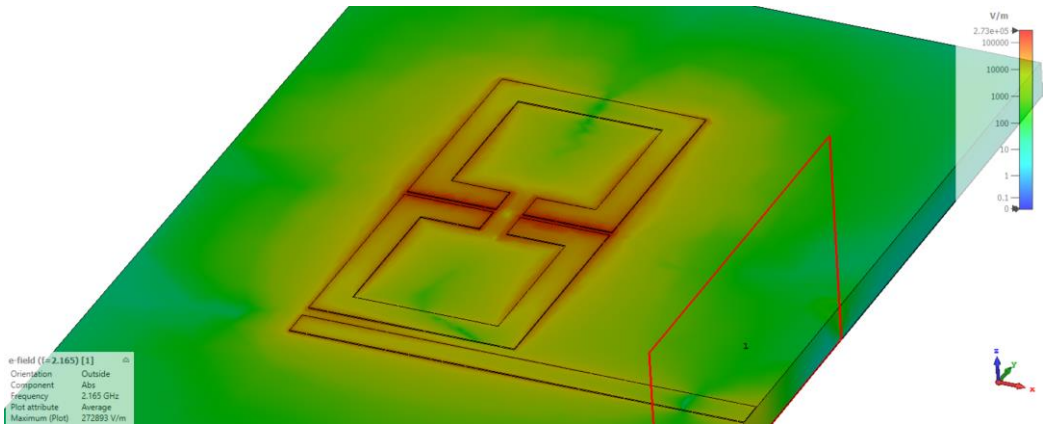

Figure 3.10. First mode 2.165 GHz E-Field plot

For the second mode at 2.59 GHz E-Field can be seen in Figure 3.11. For this mode, as seen, the electric field density exhibits the maximum values on the sides of the resonators and the gaps between the ends of the open loop resonators.

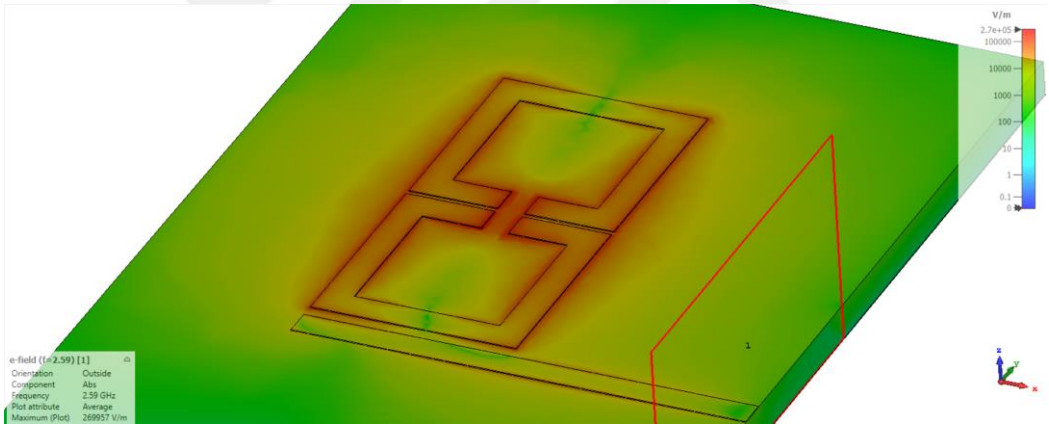

Figure 3.11. Second mode 2.59 GHz E-Field plot

These two resonance frequencies could be adjusted by changing the distance between two resonators. While adjusting frequency, the center frequency for two bands are changing because of the nature of the geometry. The relation between distance and frequency response is unique to that resonator size, and for this work, it is calculated by using curve fitting methods where the details are given in the following paragraphs..

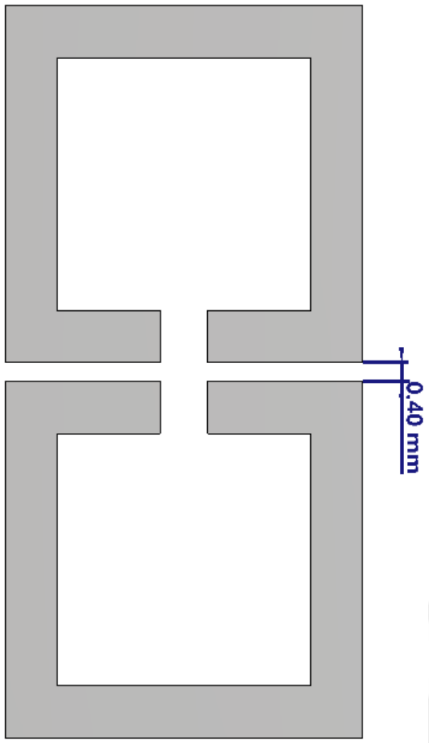

Figure 3.12. Dual mode resonator configuration and the distance between single mode resonators

Table 3.1. The relation between the distance and filter's center frequencies

Distance (mm)	**f_{c1} (GHz)**	**f_{c2} (GHz)**	**f_c (GHz)**
0.2000	2.5900	2.1650	2.3680
0.4000	2.5510	2.2400	2.3904
0.6000	2.5200	2.3000	2.4075
0.8000	2.4960	2.3280	2.4105
1.0000	2.4760	2.3520	2.4132

Using Table 3.1 inputs and curve fitting algorithm on MATLAB [23], generated polynomial can be seen in equation (3.5). This polynomial gives a center frequency that corresponds to the given distance between the resonators(d). Since this polynomial is generated by using the inputs from designed resonator, it is a unique polynomial that is only valid for designed resonator.

$$f_c(d) = 0.0521d^3 - 0.1893d^2 + 0.2191d + 2.331 \quad (3.5)$$

Fitted polynomial is plotted on Figure 3.13.

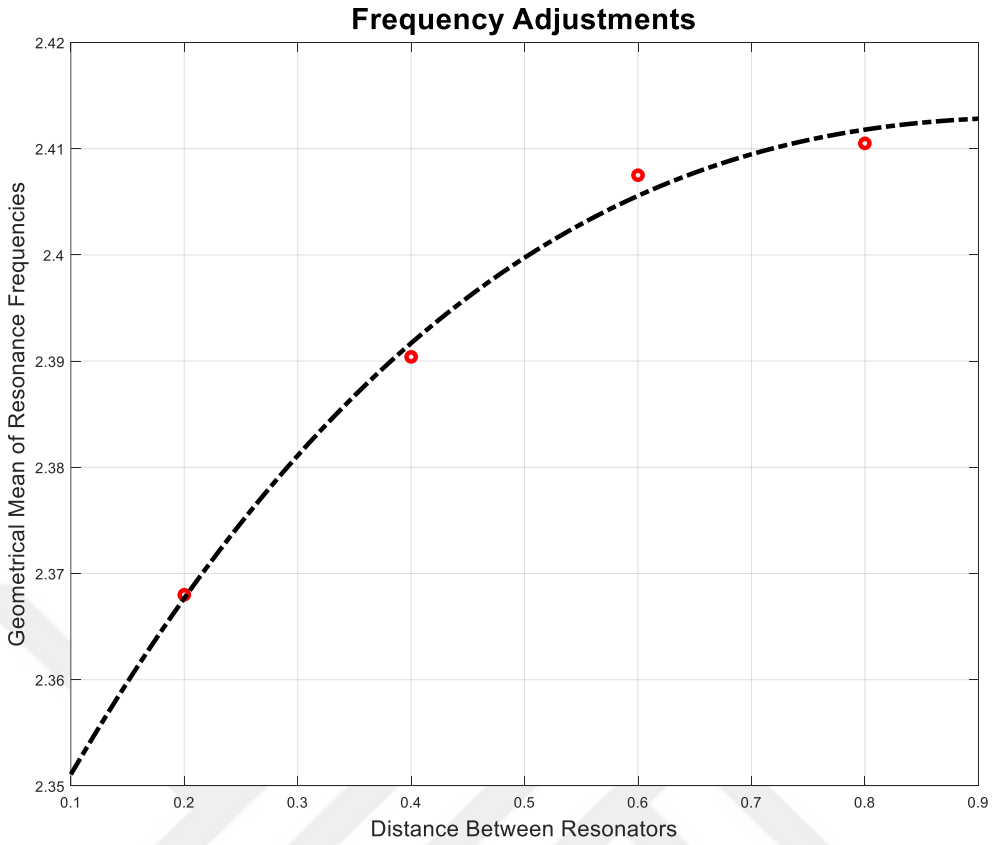

Figure 3.13. Curve fitting on the dataset of resonance frequency and distance

As seen, there are limits for this frequency adjustments and to fix f_c at the same frequency, resonator size and the distance should be adjusted at the same time.

When the frequency adjustments are finished for both bands, external Q of the feeds must be adjusted. In CST Studio Suite, by using Eigenmode solver, external quality (Q_e) factors of the resonance frequencies could be simulated. To calculate required external Q, coupling matrix **(M)** (3.6) and fractional bandwidth (FBW) (3.7) is required.

$$\mathbf{M} = \begin{bmatrix} 0 & 2.024 & 0 & 1 \\ 2.024 & 0 & 0.0001 & 0 \\ 0 & 0.0001 & 0 & 2.024 \\ 1 & 0 & 2.024 & 0 \end{bmatrix} \tag{3.6}$$

$$\mathrm{FBW} = \frac{\mathrm{BW}}{f_{c_{\mathrm{dualband}}}} = \frac{125\ \mathrm{MHz}}{\sqrt[2]{f_{c_{\mathrm{first\ band}}} * f_{c_{\mathrm{second\ band}}}}} \tag{3.7}$$

$$\mathrm{FBW} = \frac{125\ \mathrm{MHz}}{\sqrt[2]{2155\ \mathrm{MHz} * 2595\ \mathrm{MHz}}}$$

$$FBW = 0.0529$$

Required external quality factor (Q_e) of the source coupling (M_{S1}) could be calculated by using (3.8).

$$Q_e = \frac{1}{FBW * {M_{S1}}^2}$$

$$Q_e = \frac{1}{0.0529 * 2.024^2} \tag{3.8}$$

$$Q_e = 4.61$$

After calculating Q_e, the objective is to achieve required Q_e values for both resonant frequencies by adjusting the width of the feed line or the distance between feed line and first resonator.

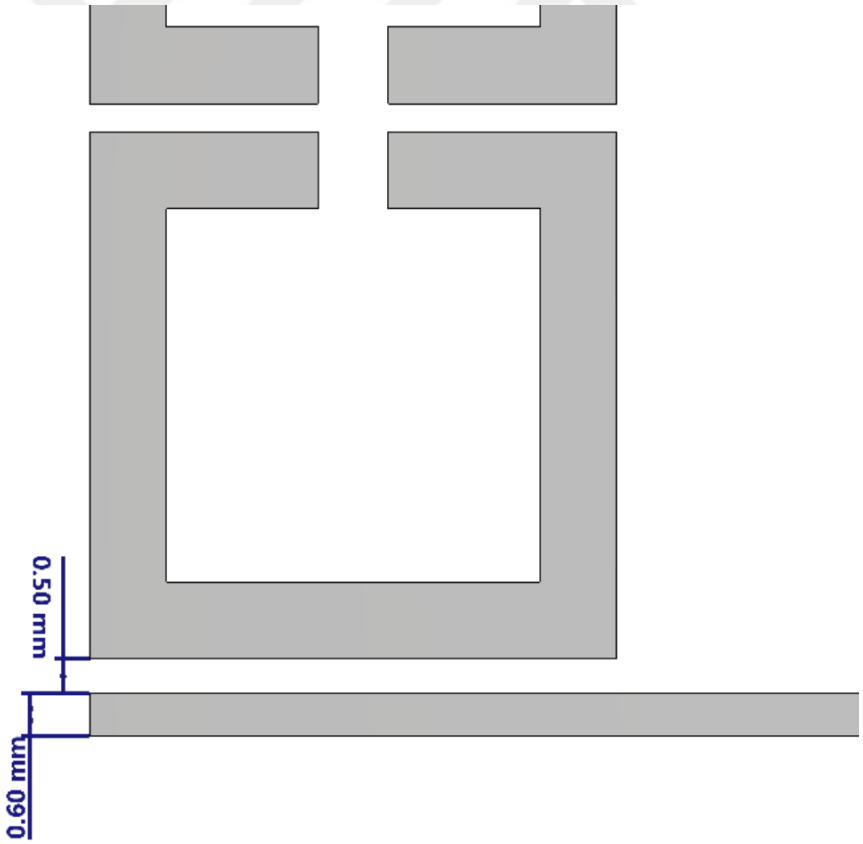

Figure 3.14. External-Q adjustments on feed

In that work, analytical [19] and simulation [20] methods are used for the calculation of the external quality factor to compare and make sure that the same results could be get

with different methods in case of having only the S parameters of the resonator and not having Eigenmode solver.

To calculate the achieved Q_e, single resonator is fed by using a coupled line which has 50 Ohm impedance at center frequency. After that, the distance between the resonator and coupled feed line could be changed to tune the external Q of the resonator. If fine tuning is needed, thickness of the coupled line is also changing the external Q factor and it can be used.

Achieved Q_e is calculated by using CST Studio Suite as below.

Mode	Loaded Frequency	External Q
4	2.161 GHz	140.3
5	2.592 GHz	79.93

Figure 3.15. Calculated External Q by using CST Studio Suite

Also achieved Q_e could be calculated by using equation (5.4) is shown before.

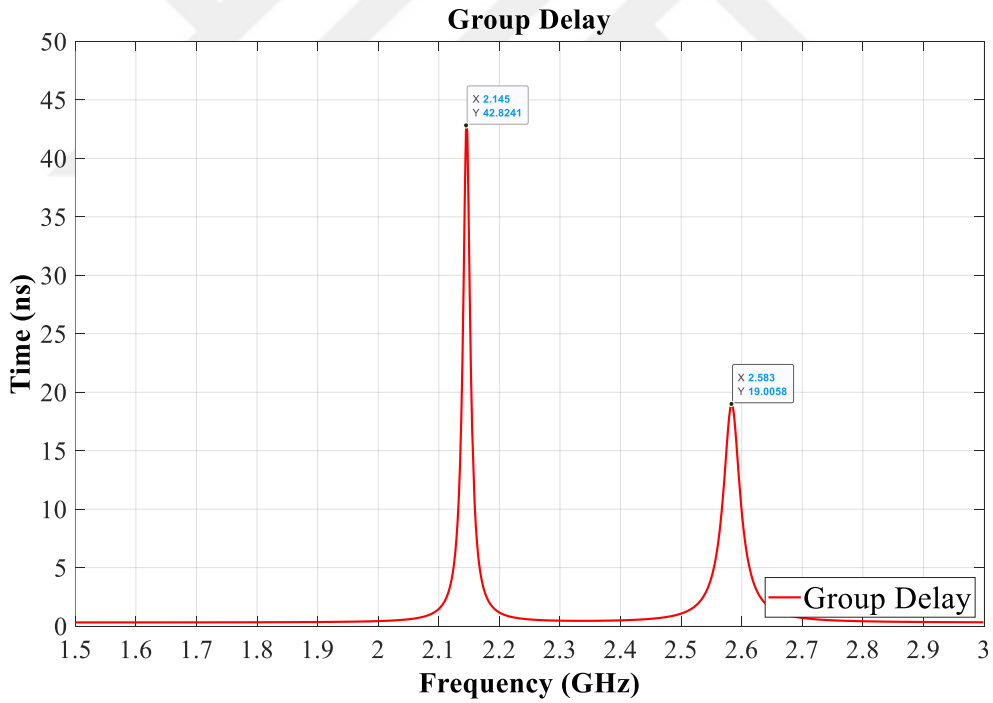

Figure 3.16. Group delay plot of single dual-mode resonator

Group delay of the S_{11} response at mode frequencies are 43 ns and 2.6 ns respectively. By using those values Q_e is calculated as 144 and 77 respectively.

Table 3.2. Comparison of two methods used for calculation of external-Q values

	Mode 1	Q_{e1}	Mode 2	Q_{e2}
Eigenmode Solver	2.161 GHz	140.3	2.592 GHz	79.9
Calculation	2.145 GHz	144	2.583 GHz	77

In this thesis, unloaded-Q is parameter is calculated by using Q-Factor Calculator of CST program. The calculated Unloaded-Q values of the first and second modes of the dual mode resonator are given in Figure 3.17 and Figure 3.18.

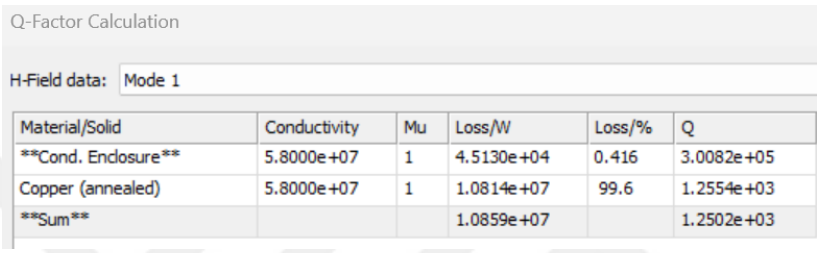
Q-Factor Calculation

H-Field data: Mode 1

Material/Solid	Conductivity	Mu	Loss/W	Loss/%	Q
Cond. Enclosure	5.8000e+07	1	4.5130e+04	0.416	3.0082e+05
Copper (annealed)	5.8000e+07	1	1.0814e+07	99.6	1.2554e+03
Sum			1.0859e+07		1.2502e+03

Figure 3.17. Unloaded-Q calculation for first mode by using CST Studio Suite

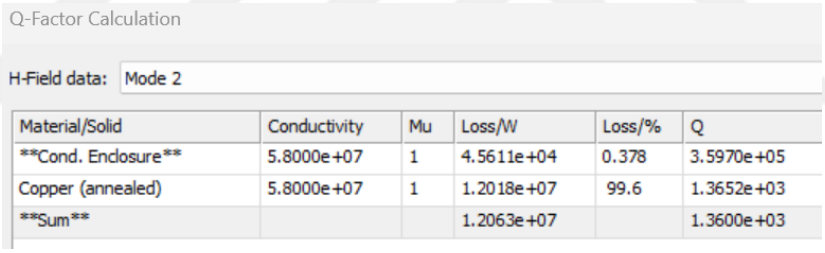
Q-Factor Calculation

H-Field data: Mode 2

Material/Solid	Conductivity	Mu	Loss/W	Loss/%	Q
Cond. Enclosure	5.8000e+07	1	4.5611e+04	0.378	3.5970e+05
Copper (annealed)	5.8000e+07	1	1.2018e+07	99.6	1.3652e+03
Sum			1.2063e+07		1.3600e+03

Figure 3.18. Unloaded-Q calculation for second mode by using CST Studio Suite

The next step is the implementation of M_{SL} coupling, source to load coupling coefficient, which is an element of the synthesized coupling matrix **M**. Since it is equal to unity, it indicates that direct source – load coupling coupling is required to implement this filter. That can be realized by implementing $\frac{\lambda}{4}$ long transmission line between source and load [24] where λ corresponds the wavelength of the center frequency of dual band resonator ($f_{c_{dualband}}$). Example implementation can be seen in Figure 3.19 below. To calculate the wavelength for microstrip, TXLINE [25] software is used, which is a package software in AWR Microwave Office.

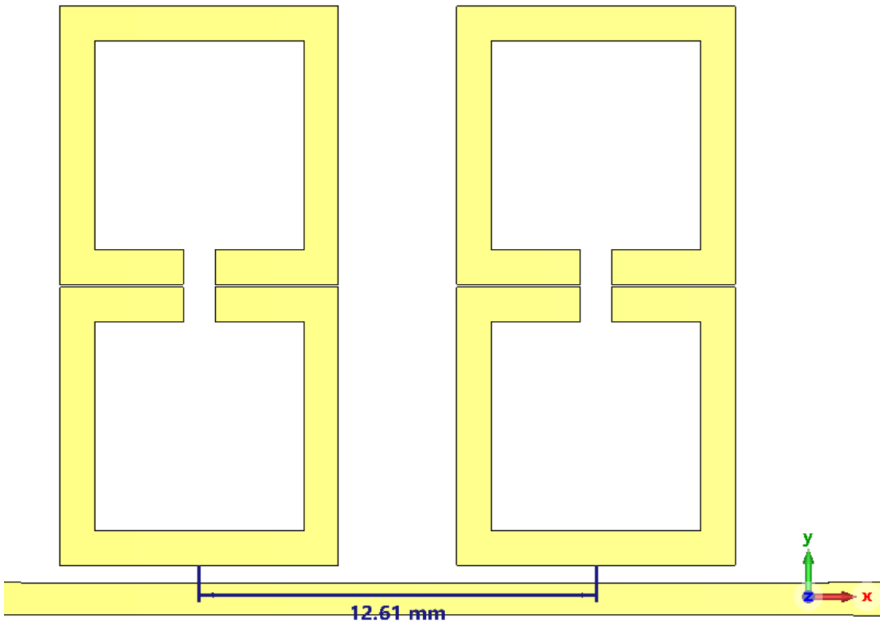

Figure 3.19. The distance between the resonators that is placed on through line

To calculate the desired physical coupling (**k**) between the resonators, synthesized coupling matrix (**M**) from equation (3.6) should be converted to the physical couplings (**k**) matrix. This conversion could be made by multiplying coupling matrix to the fractional bandwidth of the desired filter given in equation (3.7). Since the aim is to have a dual-band bandstop filter to stop the signals between 2110 MHz – 2200 MHz and 2500 MHz – 2690 MHz bands.

$$\mathbf{k} = \mathbf{M} * \mathrm{FBW}$$

$$\mathbf{k} = \begin{bmatrix} 0 & 2.024 & 0 & 1 \\ 2.024 & 0 & 0.0001 & 0 \\ 0 & 0.0001 & 0 & 2.024 \\ 1 & 0 & 2.024 & 0 \end{bmatrix} * 0.0529 \tag{3.9}$$

$$\mathbf{k} = \begin{bmatrix} 0 & 0.107 & 0 & 0.0529 \\ 0.107 & 0 & 0 & 0 \\ 0 & 0 & 0 & 0.107 \\ 0.0529 & 0 & 0.107 & 0 \end{bmatrix}$$

Since coupling between the first and the second resonator (M_{12}) is almost zero, after physical coupling matrix conversion, it converges to a negligible value, so it could be taken as zero. Still, it needs to be checked by changing the distance between the first and second resonator and measuring the coupling. The same method is going to be used while adjusting the frequencies of the bands.

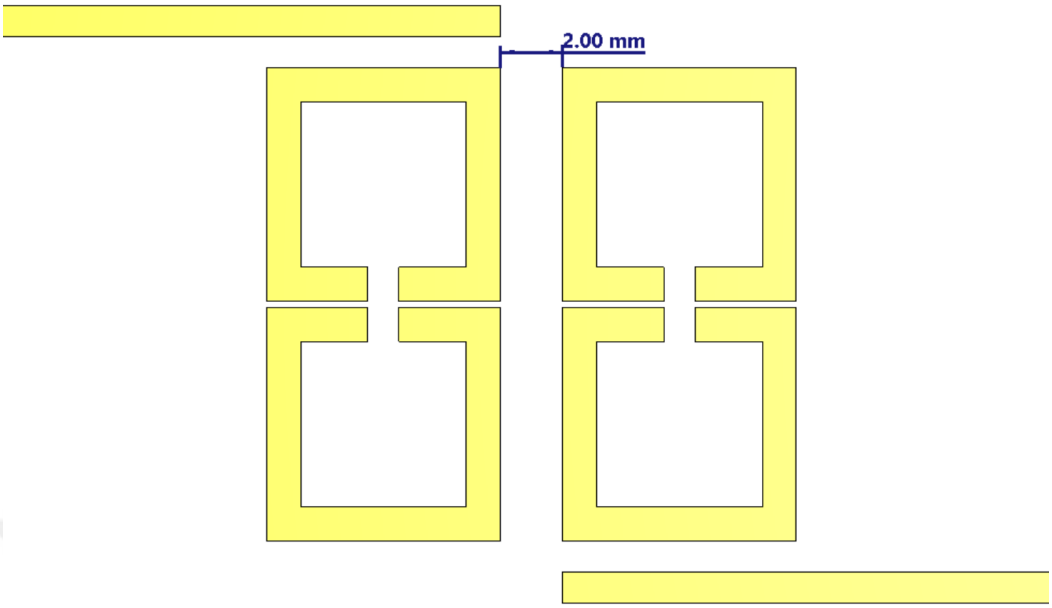

Figure 3.20. Measurement of the coupling coefficient between the coupled dual-mode resonators

After changing the distance between dual mode resonators, negligible coupling is seen after 2mm distance.

When all the calculations are made, filter could be implemented. In this work, CST Studio Suite 2021 is used for modelling and simulation of the filter response. As solver, frequency domain solver is recommended for resonant structures, but similar results could be achieved by time domain solver too. At solver settings, adaptive tetrahedral mesh refinement should be checked to have simulation results approximate to the real measurements. Frequency domain solver settings are shown in Figure 3.21.

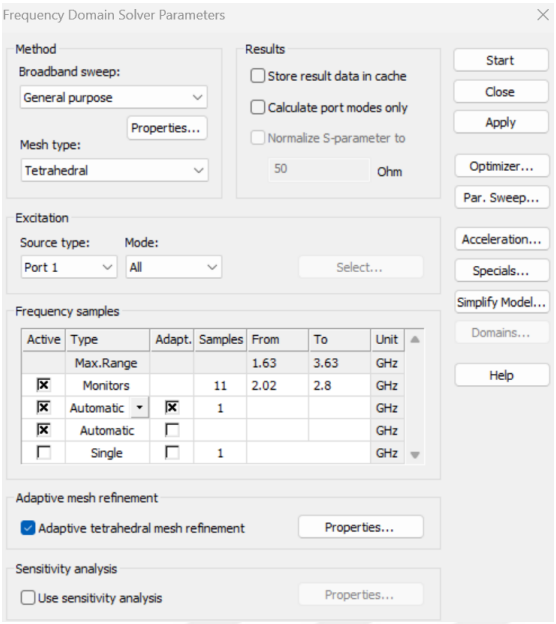

Figure 3.21. Frequency domain solver settings

Also, under "Specials" menu, solver order should be set to 3rd (High Accuracy) mode and under Equation System Solver accuracy shall be set to "1e-5" as shown in Figure 3.22.

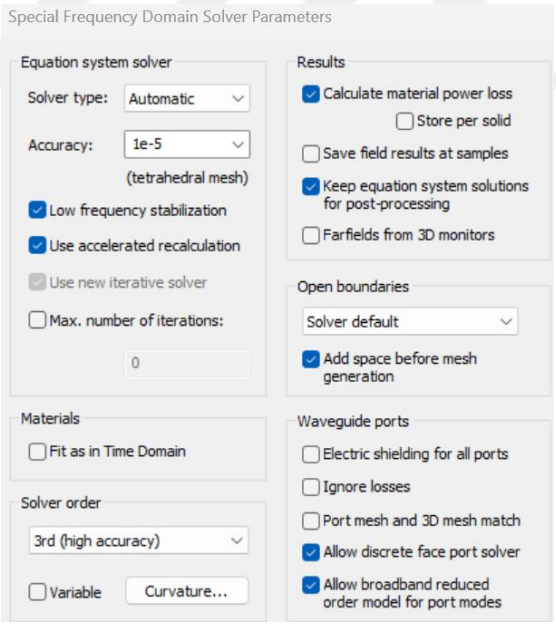

Figure 3.22. Special settings of frequency domain solver

Boundary conditions are now changed to "Open" as shown in Figure 3.23. If it is still simulated as electrical wall, to have the same frequency response after manufacturing the filter, filter must be placed in a box which is made from grounded conductor. After changing

the boundary conditions to “open”, frequency domain solver simulates the filter in open space without any effect from outside. “Open boundary box” is shown in Figure 3.24.

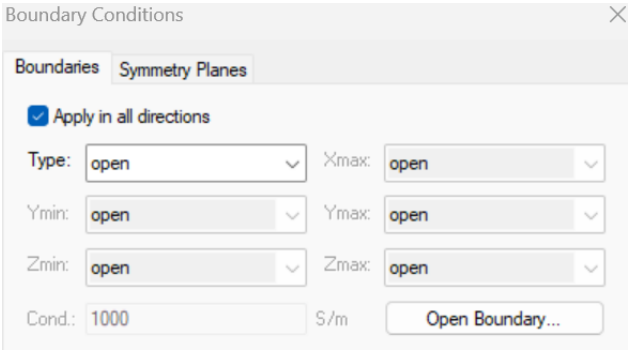

Figure 3.23. Used boundary conditions for frequency domain solver

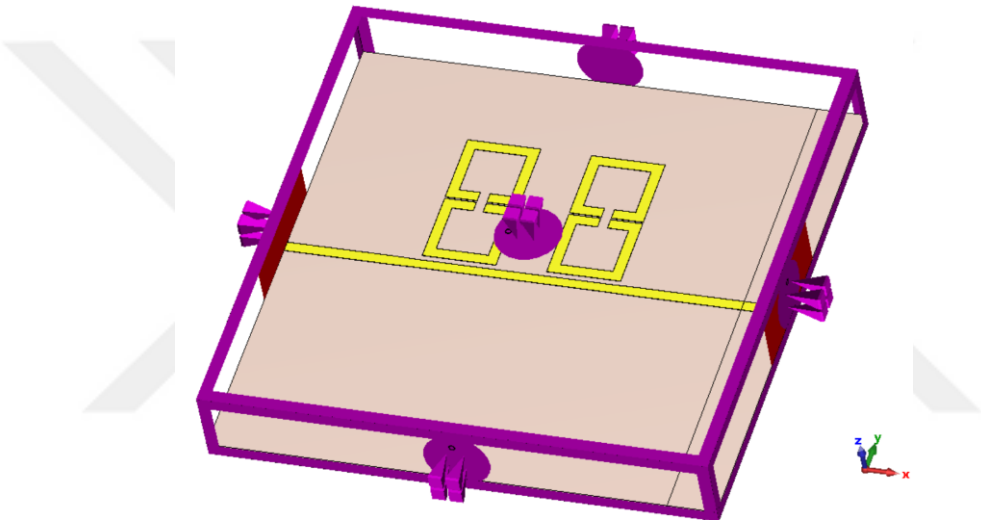

Figure 3.24. Bounding box that is used on frequency domain solver simulations

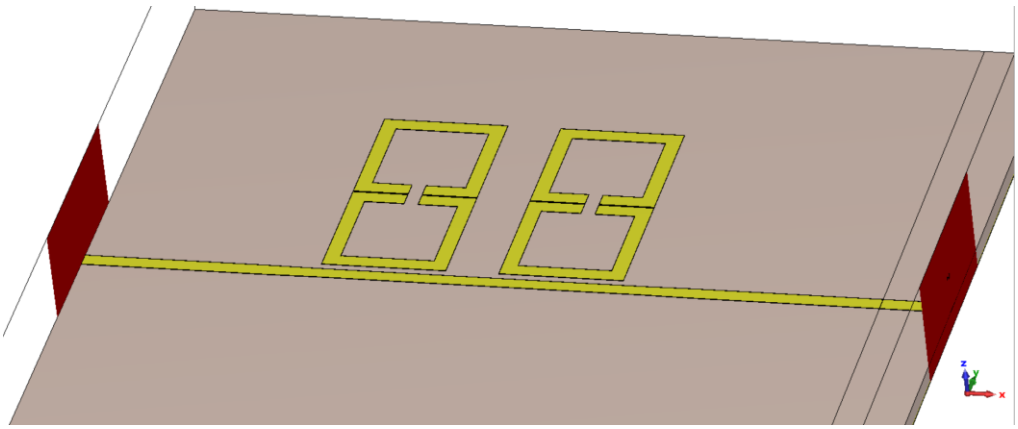

Figure 3.25. Filter with two dual mode resonators

Realized design with two resonators of the filter is shown in Figure 3.25. Simulation results are shown in Figure 3.26.

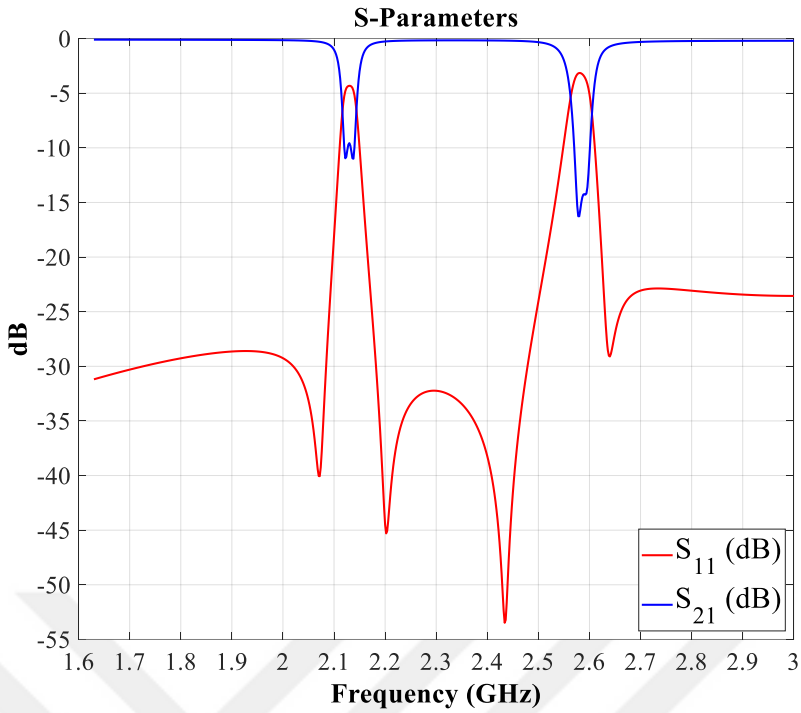

Figure 3.26. S-Parameter response graph of the designed filter

For the first band, it is centered at 2.13 GHz (25MHz shifted) and bandwidth is 40 MHz. It is shifted by 25 MHz and 50 MHz narrow than the desired response. For the second band, it is centered at 2.59 GHz and bandwidth is 56 MHz. It is exactly the desired center frequency, even though the band is still narrow than the desired value which is 200 MHz.

Since the E-Field on open loop ring resonators are fringing, at the reject band there is low reflection from input port and it is an advantage if the filter is placed at a transmitter.

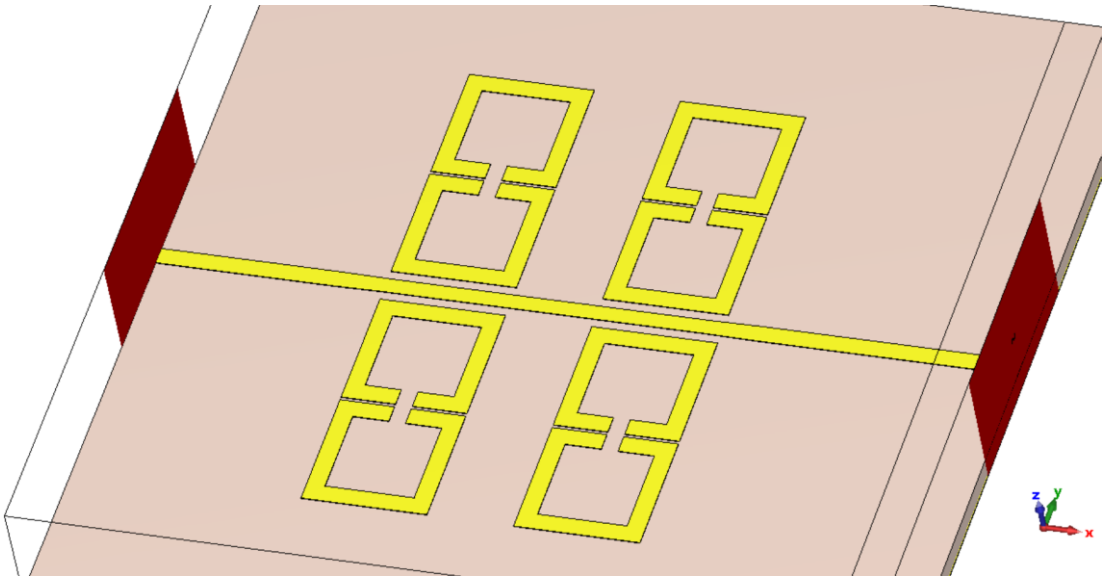

Figure 3.27. Enhanced version of the designed filter

To increase the performance of the filter, the same resonators are placed symmetrically to the opposite side of the through transmission line as seen in Figure 3.27.

Simulation is made by using the same solver settings as before. Results are shown in Figure 3.28.

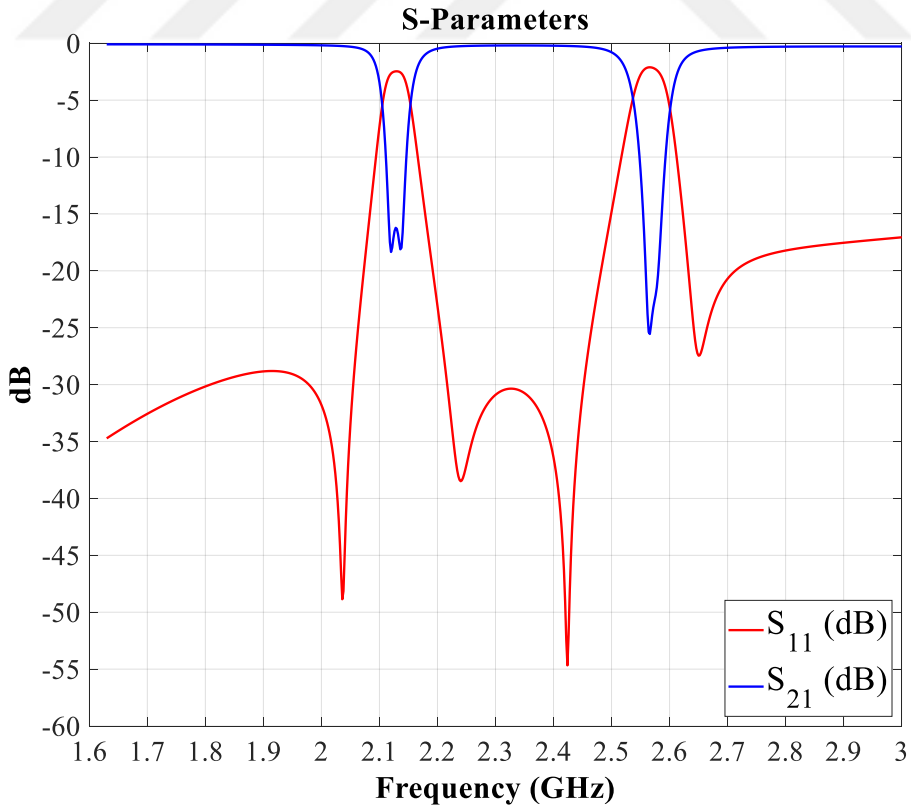

Figure 3.28. S-Parameter response of the enhanced filter

For the first band, it is centered at 2.12 GHz (24 MHz shifted) and the bandwidth is 70 MHz. It is shifted 24 MHz and 20 MHz narrow than the desired response. For the second band, it is centered at 2.56 GHz and bandwidth is 90 MHz. It is almost the desired center frequency, even though the band is still narrow than the desired value which is 200 MHz. As overall, better RF performance is achieved by placing symmetrical design to the other side of the through transmission line.

While adding symmetrical resonators to the other side of the through transmission line, external quality factor of the resonators is changed since the resonators are coupled from the same point of the transmission line. Q_e adjustments are required to have better results. Distance between the resonators and through line is changed from 0.55 to 0.2 to adjust Q_e and simulation is made again. Results are shown in Figure 3.29.

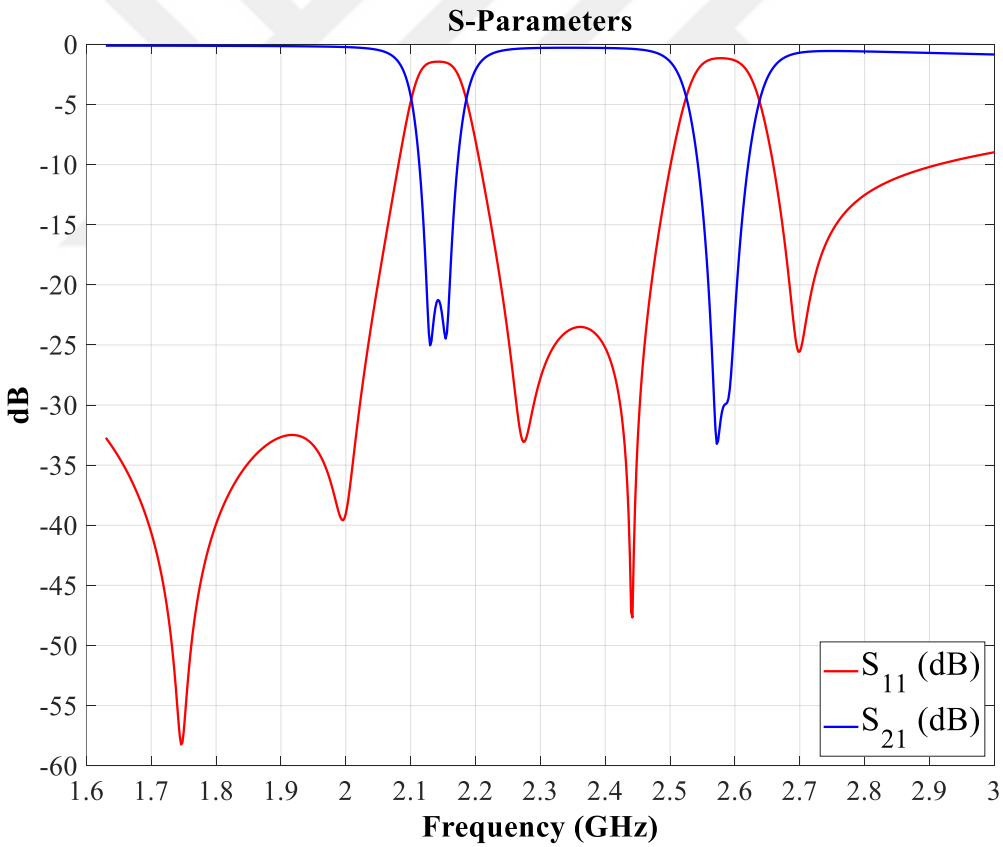

Figure 3.29. S-Parameter response of the enchanced filter after external-Q correction

As seen in Figure 3.29, the first band is centered at 2.14 GHz and bandwidth is 100 MHz. The second band is centered at 2.58 GHz and bandwidth is 132 MHz. First band complies with the requirement but the second band is still narrower than required. Since the

order of the filter is the same for both bands, increasing second band's width will cause the same effect on first band. For this case, it is an undesired effect to not to lose signals that comes close to the first band. As a result, the design is completed at that point while compromising from second band bandwidth goal.

Also, if frequency tuning is needed for two bands, it can be tuned by changing the distance of two combined single mode resonators that used in a stacked way. The parameter sweep is shown in Figure 3.30.

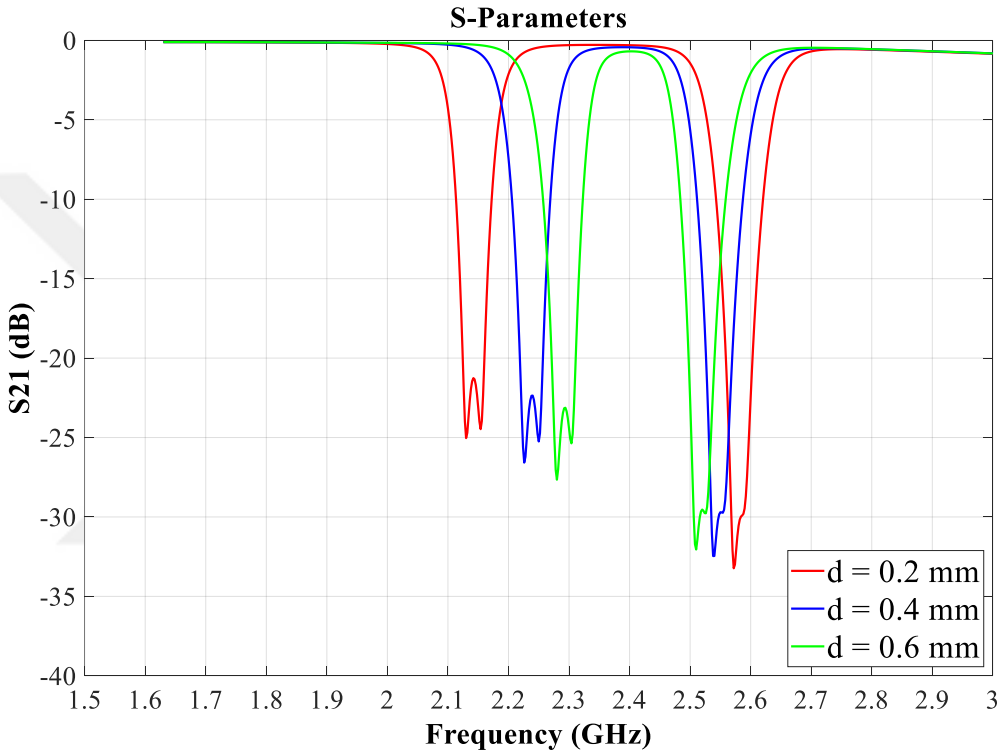

Figure 3.30. The change of band frequencies due to the change of the distance between single mode open-loop resonators

Until this section, filter is designed by using RT/Duroid 6010 substrate, which offers less insertion loss due to lower tangent loss and more compact size due to its higher $\varepsilon_r = 10.7$. However, the more cost-effective FR-4 material was preferred in the manufacturing process. The FR-4 material is commonly preferred material in the manufacturing of radio frequency components due to its low cost and widespread use. As a result, compared to the design with RT/Duroid 6010, the same coupling matrix is utilized for the realization of filter by FR-4 substrate. Since the thickness and ε_r of FR-4 are changed; resonator dimensions,

impedances and Q values are recalculated. Designed filter with its new dimensions is shown in Figure 3.31.

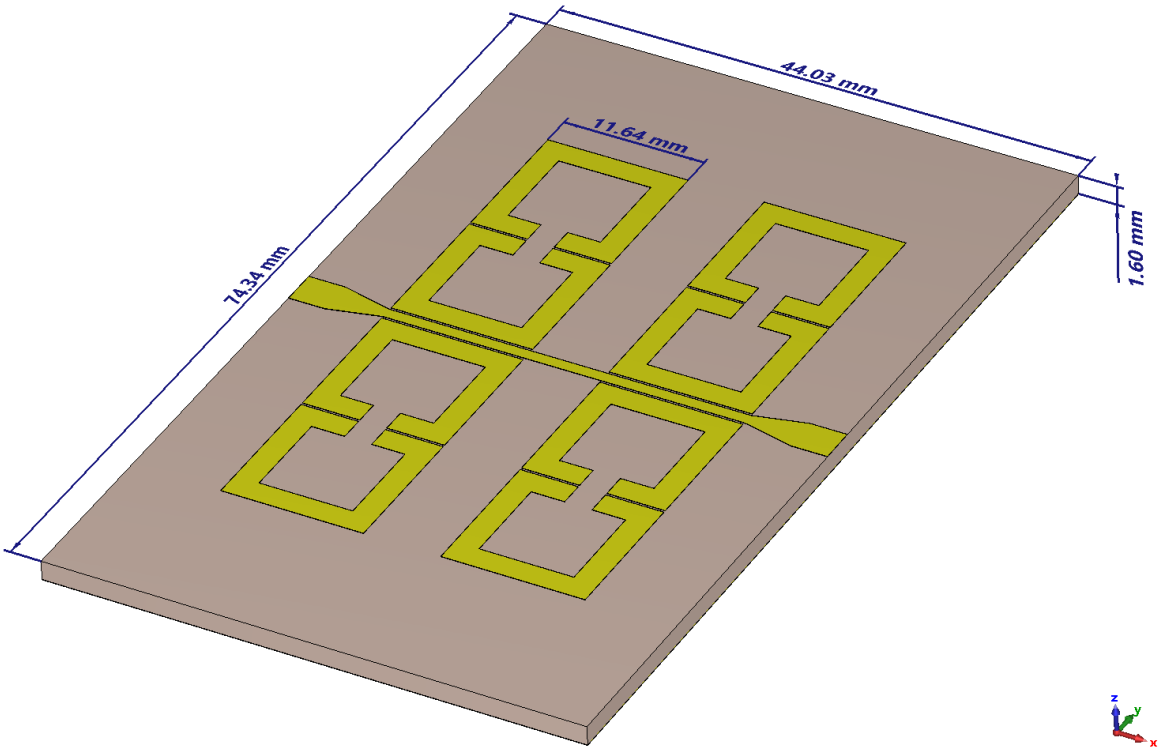

Figure 3.31. The version that is designed on FR-4 substrate

The S-Parameter results of the filter on FR-4 substrate are shown in Figure 3.32.

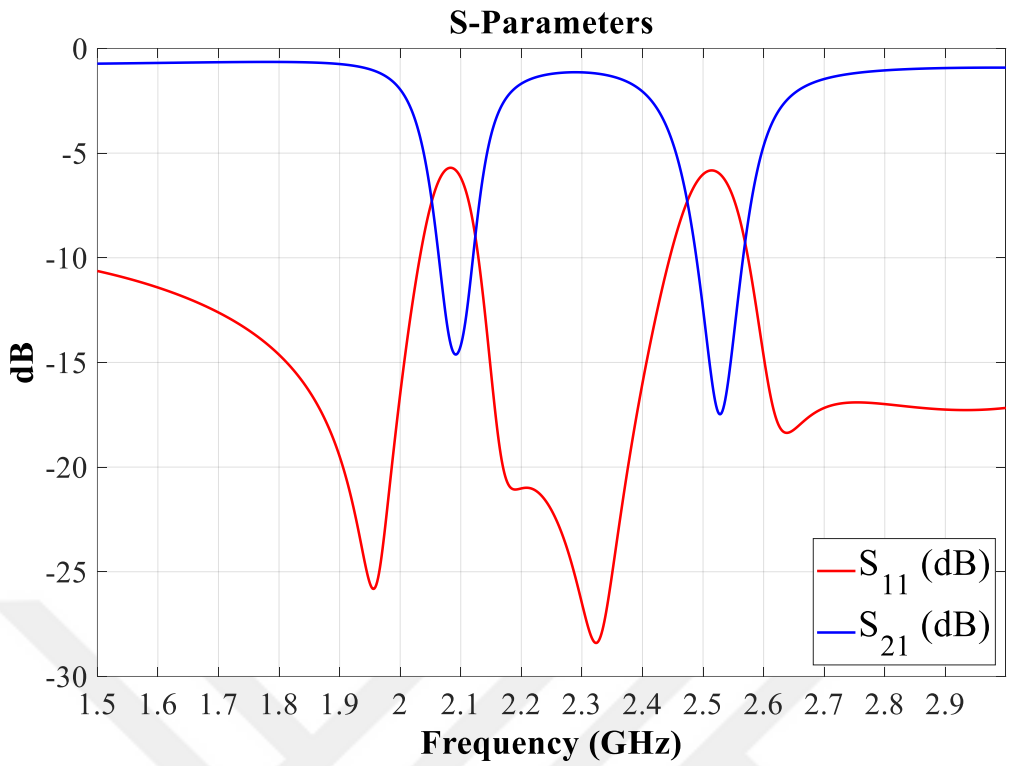

Figure 3.32. S-Parameter response of the FR-4 version of the filter

For the first band, it is centered at 2.1 GHz and bandwidth is 150 MHz. For the second band, it is centered at 2.5 GHz and bandwidth is 200 MHz. FR-4 substrate has 0.025 tangent loss value, and it is thicker. Tangent loss and substrate thickness are higher than Rogers RT/Duroid 6010 substrate which is used on earlier designs. These differences cause higher insertion losses. As a result of higher losses, bandwidths are larger, and at the stop bands S_{11} (Port reflection) is lower as seen in Figure 3.32. Low reflections might be beneficial if the filter is used on transmit cases, but it is not in the scope of this work.

4.MEASUREMENTS OF THE PROPOSED FILTER

Figure 4.1. Manufactured FR-4 Filter

The manufactured filter is shown in Figure 4.1. HASL (Hot Air Solder Levelling) with lead surface finishing is applied to copper traces to prevent copper from oxidation. This process is not recommended for higher frequency designs because of the additional roughness effect on the surface.

Filter response is measured by using Keysight PNA-X N5242A Network Analyzer and results are shown as comparison between measurement and simulation in Figure 4. 2.

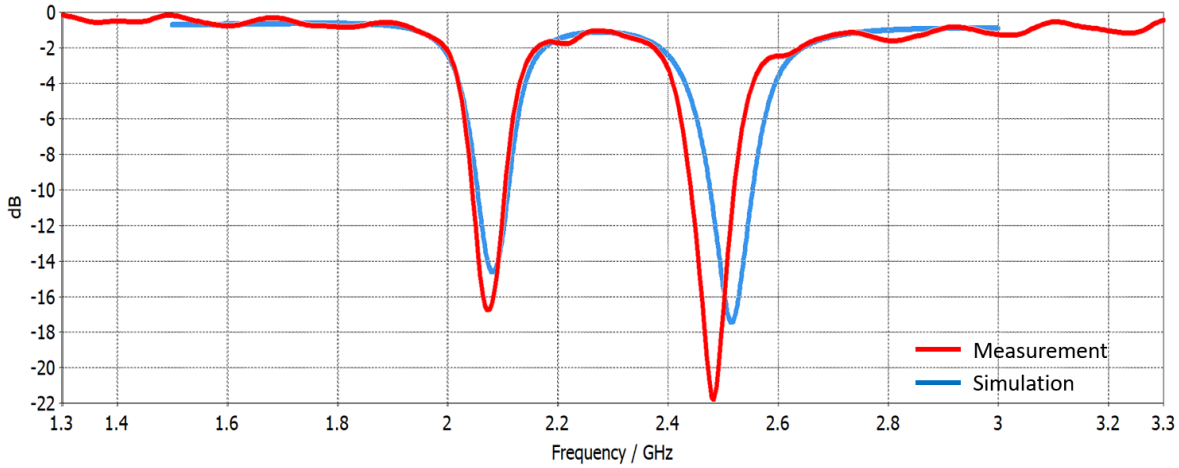

Figure 4. 2 Comparison of simulation and measurement results

As seen in Figure 4. 2, for the first band, it is centered at 2.08 GHz and bandwidth is 130 MHz. Achieved center frequency is the same with the simulation but, bandwidth is 13 MHz narrower than the expected response. For the second band, it is centered at 2.5 GHz and bandwidth is 170 MHz. Achieved center frequency is shifted by 10 MHz and, bandwidth is 30 MHz narrower than the expected response. Insertion loss is almost the same with simulations except the small ripple on the measurement.

5. CONCLUSION

This thesis introduces a novel approach for the design of a dual-band bandstop filter. By using the Square Open-Loop resonators in a grouped manner, the proposed method enables designers to use a single band bandstop filter coupling matrix $(N + 2) \times (N + 2)$ rather than a dual band bandstop coupling matrix $(2N + 2) \times (2N + 2)$. The physical configuration can be implemented using solely a single-band bandstop filter coupling matrix, which is also more straightforward to synthesize and use compared to dual-band coupling matrix. Additionally, by using this technique, the length of the through line on the filter is reduced in half that also helps reducing the insertion loss, which becomes more significant at higher frequencies. It also enables low-frequency filters to have lower dimensions and high-frequency filters to be manufactured with lesser effort since the resonator's dimensions lay between those of a low-frequency and a high-frequency single-mode resonator. The method developed in this study provides designers the opportunity to implement more compact designs for low-frequency and ease of manufacturing for high-frequency designs.

The novel method developed in this study was applied to design a filter that suppresses frequencies between 2110 MHz-2200 MHz and 2500 MHz-2690 MHz. A coupling matrix is initially created and tuned. An appropriate layout and resonator were then selected. The desired coupling matrix properties are obtained by designing the filter on simulation software by using proposed resonators in the required architecture. Due to its better RF characteristics and high-quality manufacturing process, RT/Duroid 6010 has been utilized in simulation to demonstrate the proposed layout's remarkable potential for cutting-edge applications. Another filter with the same layout configuration is designed and manufactured using FR-4 substrate to verify the simulation with the measurements. Even though the FR-4 substrate used has poor performance at frequencies higher than 1GHz, measurements revealed acceptable discrepancies. Further iterations can be performed to achieve the more precise RF performance since FR-4 substrate is a low-cost manufacturing choice. The simulations and the created filter provide proof for the novel realization technique.

REFERENCES

[1] P. Apostolov, A. Meklyov and V. Kostov, "Band-pass and Band-stop Filters Synthesis Using Sigmoidal Function," 2021 *12th National Conference with International Participation (ELECTRONICA)*, 2021, pp. 1-3, doi: 10.1109/ELECTRONICA52725.2021.9513699..

[2] P. Chomtong and P. Akkaraekthalin, "A dual-band cavity bandpass filter using interdigital technique," 2017 *IEEE Conference on Antenna Measurements & Applications (CAMA)*, Tsukuba, Japan, 2017, pp. 261-264, doi: 10.1109/CAMA.2017.8273419.

[3] H. Miyake, S. Kitazawa, T. Ishizaki, T. Yamada and Y. Nagatomi, "A miniaturized monolithic dual band filter using ceramic lamination technique for dual mode portable telephones," 1997 *IEEE MTT-S International Microwave Symposium Digest*, Denver, CO, USA, 1997, pp. 789-792 vol.2, doi: 10.1109/MWSYM.1997.602908.

[4] Azad, Amit Ranjan & Jhariya, Dharmendra & Mohan, Akhilesh. (2018). Substrate-integrated waveguide cross-coupled filters with mixed electric and magnetic coupling structure. *International Journal of Microwave and Wireless Technologies.* 10. 1-8. 10.1017/S1759078718000843.

[5] C. Karpuz, A. Görür, E. Güntürkün and A. K. Görür, "Asymmetric response dual-mode dual-band bandstop filters having simple and understandable topology," 2009 *Asia Pacific Microwave Conference*, Singapore, 2009, pp. 925-928, doi: 10.1109/APMC.2009.5384319.

[6] Chavda, K., Sarvaiya, A.K. (2023). Design and Analysis of Band Stop Filter Using Hexagonal Split Ring Resonator for Wireless Application. In: Kaiser, M.S., Xie, J., Rathore, V.S. (eds) *Information and Communication Technology for Competitive Strategies* (ICTCS 2021)

[7] ÇINAR, Alparslan & BİÇER, Sinan. (2020). Band-stop filter design based on split ring resonators loaded on the microstrip transmission line for GSM-900 and 2.4 GHz ISM band. *International Advanced Researches and Engineering Journal*. 29-33. 10.35860/iarej.641459.

[8] Asci, Cihan & Sadeqi, Aydin & Wang, Wei & Rezaei Nejad, Hojatollah & Sonkusale, Sameer. (2020). Design and implementation of magnetically–tunable quad–band filter utilizing split–ring resonators at microwave frequencies. *Scientific Reports*. 10. 10.1038/s41598-020-57773-6.

[9] Awasthi, S., Biswas, A. and Akhtar, M.J. (2015), Dual-band dielectric resonator bandstop filters. *Int J RF and Microwave Comp Aid Eng*, 25: 282-288. https://doi.org/10.1002/mmce.20860

[10] Jia-Sheng Hong and M. J. Lancaster, "Couplings of microstrip square open-loop resonators for cross-coupled planar microwave filters," in *IEEE Transactions on Microwave Theory and Techniques*, vol. 44, no. 11, pp. 2099-2109, Nov. 1996, doi: 10.1109/22.543968.

[11] K. Lee, T. -H. Lee, C. -S. Ahn, Y. -S. Kim and J. Lee, "Reconfigurable Dual-Stopband Filters With Reduced Number of Couplings Between a Transmission Line and Resonators," in *IEEE Microwave and Wireless Components Letters*, vol. 25, no. 2, pp. 106-108, Feb. 2015, doi: 10.1109/LMWC.2014.2382659.

[12] R. J. Cameron, "General coupling matrix synthesis methods for Chebyshev filtering functions," in *IEEE Transactions on Microwave Theory and Techniques*, vol. 47, no. 4, pp. 433-442, April 1999, doi: 10.1109/22.754877.

[13] Richard J. Cameron; Chandra M. Kudsia; Raafat R. Mansour, "Synthesis of a General Class of the Chebyshev Filter Function," in *Microwave Filters for Communication Systems: Fundamentals, Design, and Applications* , Wiley, 2018, pp.177-213, doi: 10.1002/9781119292371.ch6.

[14] Richard J. Cameron; Chandra M. Kudsia; Raafat R. Mansour, "Synthesis of Networks: Direct Coupling Matrix Synthesis Methods," in *Microwave Filters for Communication Systems: Fundamentals, Design, and Applications* , Wiley, 2018, pp.247-294, doi: 10.1002/9781119292371.ch8.

[15] R. J. Cameron, "Advanced Filter Synthesis," in *IEEE Microwave Magazine*, vol. 12, no. 6, pp. 42-61, Oct. 2011, doi: 10.1109/MMM.2011.942007.

[16] Corrales, Eden & de Paco, Pedro & Menendez, Oscar. (2011). Direct coupling matrix synthesis of bandstop filters. *Progress In Electromagnetics Research Letters*. 27. 85-91. 10.2528/PIERL11091512.

[17] Z. N. He, X. L. Wang, S. H. Han, T. Lin & Z. Liu (2008) The Synthesis and Design for New Classic Dual-Band Waveguide Band-Stop Filters, *Journal of Electromagnetic Waves and Applications*, 22:1, 119-130, DOI: 10.1163/156939308783122689

[18] Richard J. Cameron; Chandra M. Kudsia; Raafat R. Mansour, "Design and Physical Realization of Coupled Resonator Filters," in *Microwave Filters for Communication Systems: Fundamentals, Design, and Applications* , Wiley, 2018, pp.457-484, doi: 10.1002/9781119292371.ch14.

[19] Jia-Sheng Hong; M.J. Lancaster, "Coupled Resonator Circuits, " in *Microstrip Filters for RF/Microwave Applications*, Wiley, 2001, pp.235-272, doi:10.1002/0471221619.ch8

[20] Dassault Systemes, Velizy-Villacoublay, France. *CST Studio Suite 2022*. Accessed: [Online]. Available: 3ds.com/products-services/simulia/products/cst-studio-suite/

[21] Richard J. Cameron; Chandra M. Kudsia; Raafat R. Mansour, "Microwave Resonators," in *Microwave Filters for Communication Systems: Fundamentals, Design, and Applications* , Wiley, 2018, pp.373-394, doi: 10.1002/9781119292371.ch11.

[22] SynMatrix Technologies Inc., Toronto, Canada. *SynMatrix (2018)*. Accessed: Oct. 4, 2022. [Online]. Available: synmatrixtech.com/product

[23] MathWorks, Massachusetts, USA. *MATLAB R2022b*. Accessed: [Online]. Available: mathworks.com/products/matlab.html

[24] Richard J. Cameron; Chandra M. Kudsia; Raafat R. Mansour, "Synthesis and Application of Extracted Pole and Trisection Elements," in *Microwave Filters for Communication Systems: Fundamentals, Design, and Applications* , Wiley, 2018, pp.323-372, doi: 10.1002/9781119292371.ch10.

[25] Cadence, California, USA. *AWR TX-LINE*. Accessed: [Online]. Available: cadence.com/ko_KR/home/tools/system-analysis/rf-microwave-design/awr-tx-line.html